Stretch-Based Hyperelastic Material Formulations for Isogeometric Kirchhoff-Love Shells

Hugo M. Verhelst, Matthias M. Möller, Henk J den Besten, Angelos Mantzaflaris, Mirek L. Kaminski

Stretch-Based Hyperelastic Material Formulations for Isogeometric Kirchhoff-Love Shells

H.M. Verhelst[a,b,*], M. Möller[b], J.H. Den Besten[a], A. Mantzaflaris[c], M.L. Kaminski[a]

[a] *Delft University of Technology, Department of Maritime and Transport Technology, Mekelweg 2, Delft 2628 CD, The Netherlands*

[b] *Delft University of Technology, Department of Applied Mathematics, Van Mourik Broekmanweg 6, Delft 2628 XE, The Netherlands*

[c] *Inria Sophia Antipolis - Méditerranée, Université Côte d'Azur 2004 route des Lucioles - BP 93, 06902 Sophia Antipolis cedex, France*

Abstract

A stretch-based hyperelastic material formulation for isogeometric Kirchhoff-Love shells is presented, particularly useful when experimental material data fitting is involved to capture the model parameters, for instance using the Ogden material model. Complementing the existing invariant-based formulation, the stretch-based stress and material tensors are expressed in spectral form and transformed to the covariant curvilinear bases for consistency with the variational formulation. For both compressible and incompressible material formulations, analytical and numerical benchmarks show excellent results. In particular, the response of a collapsing conical shell - a complex collapsing mechanism - was revealed when using the arc-length method.

Keywords: Isogeometric Analysis, Kirchhoff-Love Shell, Stretch-Based Strain Energy Density Function, Arc-Length Methods

1. Introduction

To model thin shells or membranes that undergo large strains, nonlinear material relations are required, rather than the commonly used Saint Venant-Kirchhoff model. Nonlinear material models (i.e. constitutive relations) are often called *(finite) hyperelastic* models. In general, one distinguishes between phenomenological continuum mechanics approaches and molecular statistical approaches [1], which can both be described in terms of *invariants* or *principal stretches* of the deformation. Phenomenological material models include the well-known neo-Hookean, Mooney-Rivlin and Ogden material models, and statistical ones are for example the Wang-Guth and Arruda-Boyce models [1]. Numerical implementation of invariant-based material models require a less extensive computational procedure than stretch-based formulations, since principal stretches and their directions do not have to be computed. On the other hand, stretch-based descriptions can be very useful when experimental data fitting is required to capture the model

*Corresponding Author.

Email addresses: h.m.verhelst@tudelft.nl (H.M. Verhelst), m.moller@tudelft.nl (M. Möller), henk.denbesten@tudelft.nl (J.H. Den Besten), angelos.mantzaflaris@inria.fr (A. Mantzaflaris)

parameters [2–4], for instance for materials like rubber.

To model hyperelastic behavior of thin shells thin membranes, invariant-based and stretch-based formulations for Finite Element Methods (FEM) have been established [5–9]. As an alternative to thin shells in FEM, the isogeometric Kirchhoff-Love shell formulation is a well-established formulation for thin shells in the context of isogeometric analysis (IGA) [10–12]. Isogeometric Analysis [13] employs spline basis functions, providing higher continuity across basis functions. The isogeometric Kirchhoff-Love shell formulation is based on the global C^1 continuity of the isogeometric basis functions that provides a rotation-free formulation of the shell kinematics. A hyperelastic isogeometric shell formulation has been developed for general compressible and incompressible material models [12] and specific formulations for biological membranes have been obtained [14]. Dedicated approaches haven been established in order to prevent for numerical thickness integration [15]. Isogeometric Kirchhoff-Love shell formulations are successfully used for biomedical applications to model aortic valve closure [16] and bioprosthetic heart valve dynamics [17–21] as well as for industrial applications to perform buckling, vibration and nonlinear deformation analyses of composite wind turbine blade [22, 23]. All formulations [12, 14–17, 22] are invariant-based, meaning that implementation of - computationally more expensive - stretch-based models is not possible.

However, aiming to be able to use data fitted material models, finite hyperelasticity formulations in isogeometric Kirchhoff-Love shells for stretch-based (in)compressible material models are presented. The formulations are more general than the existing invariant-based formilations from [12] since invariants can be written in terms of stretches. However, the formulations in the present paper are computationally more expensive, thus complementing the invariant-based material models [12].

Following the introduction of notations, preliminary identies and the isogeometric Kirchhoff-Love shell formulation backgrounds (Section 2), the invariant-based isogemetric Kirchhoff-Love shell formulations for hyperelastic (in)compressible material models [12] are recapitulated first (Section 3). The stretch-based formulations including numerical procedures (Section 4) and the isogeometric Kirchhoff-Love shell implementation aspects (Section 5) are benchmarked with analytical or reference solutions, including an example of a collapsing conical shell (Section 6). Conclusions complete the presented work (Section 7).

2. The Kirchhoff-Love Shell Model

Using continuum mechanics and tensor calculus [24–26], the isogeometric Kirchhoff-Love formulations [10, 12, 15, 27] are briefly summarized. For more details and elaborate derivations reference is made to previous publications.

Firstly, Section 2.1 provides the notations that are used in this paper, as well as some preliminary tensor identities. Section 2.2 introduces the coordinate system and consequently the curvilinear basis that are used for the Kirchhoff-Love shell formulation. In Section 2.3 we provide the formulations of the shell kinematics, where the concepts of deformation and strain are defined. Lastly, Section 2.4 provides the variationel formulation of the Kirchhoff-Love shell, without specifying the constitutive relations, since those are covered in subsequent Sections 3 and 4.

2.1. Notations and Preliminary Identities

For the ease of reference, the notations and preliminary identities are based on the ones used by [12]. Lower-case italic quantities (a) represent scalars, lower-case bold quantities ($\mathbf{a}$) denote vectors. Upper-case quantities denote two-dimensional quantities; italic and non-bold (A) for matrices, italic and bold for second-order tensors ($\boldsymbol{A}$). Fourth-order tensors are represented by calligraphic capitals ($\mathbb{A}$). The following products operators are defined: inner product $\mathbf{a} \cdot \mathbf{b}$, cross-product $\mathbf{a} \times \mathbf{b}$ and tensor product $\mathbf{a} \otimes \mathbf{b}$. Furthermore, we represent covariant basis vectors with subscripts ($\mathbf{a}_i$) and contravariant vectors with superscript ($\mathbf{a}^j$). Latin indices take values $\{1, 2, 3\}$ whereas Greek ones take values $\{1, 2\}$. By construction, $\mathbf{a}_i \cdot \mathbf{a}^j = \delta_i^j$, with δ_i^j the Kronecker delta. Second- and fourth-order tensors are denoted by $\boldsymbol{A} = A^{ij}\, \mathbf{a}_i \otimes \mathbf{a}_j = A_{ij}\, \mathbf{a}^i \otimes \mathbf{a}^j$ and $\mathbb{A} = \mathbb{A}^{ijkl}\, \mathbf{a}_i \otimes \mathbf{a}_j \otimes \mathbf{a}_k \otimes \mathbf{a}_l = \mathbb{A}_{ijkl}\, \mathbf{a}^i \otimes \mathbf{a}^j \otimes \mathbf{a}^k \otimes \mathbf{a}^l$, respectively, where A_{ij} and $\mathbb{A}_{ijkl}$ denote covariant components and A^{ij} and $\mathbb{A}^{ijkl}$ denote contravariant components.

The Einstein summation convention is adopted to represent tensor operations. In this notation, the trace and determinant of a tensor are defined as follows for tensor $\mathbf{A} = A_{ij}\, \mathbf{a}^i \otimes \mathbf{a}^j$ as [12, 24, 25]

$$\operatorname{tr} \boldsymbol{A} = A_{ij} a^{ij} \quad \text{and} \quad \det\{\boldsymbol{A}\} = \frac{\left|A_{ij}\right|}{\left|a_{ij}\right|} \tag{1}$$

Where $\left|A_{ij}\right|$ denotes the determinant of the matrix A. The inverse of a tensor $\boldsymbol{A}$ is denoted by $\boldsymbol{A}^{-1}$ or $\bar{\boldsymbol{A}}$. The derivative of the inverse and the determinant of a tensor, with respect to one of its components become:

$$\frac{\partial \operatorname{tr} \boldsymbol{A}}{\partial A_{ij}} = a^{ij}, \quad \frac{\partial \det\{\boldsymbol{A}\}}{\partial A_{ij}} = \det\{\boldsymbol{A}\} \bar{A}_{ij} \quad \text{and} \quad \frac{\partial \bar{\boldsymbol{A}}}{\partial A_{ij}} = -\frac{1}{2}\left\{A^{-1}_{ik} A^{-1}_{lj} + A^{-1}_{il} A^{-1}_{kj}\right\}. \tag{2}$$

2.2. Shell Coordinate System

The Kirchhoff-Love shell element formulation is based on the Kirchhoff Hypothesis, that is, the cross-section does not shear and orthogonal vectors in the undeformed configuration remain orthogonal after deformation. As a consequence, any point in the shell can be represented by a point on the mid-surface and a contribution in normal direction:

$$\mathbf{x} = \mathbf{r} + \theta^3 \mathbf{n}, \tag{3}$$

with the shell mid-surface by $\mathbf{r}(\theta^1, \theta^2)$ and the unit normal direction $\mathbf{n}(\theta^3)$ for the deformed configuration $\mathbf{x}(\theta^1, \theta^2, \theta^3)$. For the undeformed configuration $\mathring{\mathbf{x}}$, the same relation holds with all quantities decorated with a $\mathring{\cdot}$. The parametrization utilizes surface coordinates θ^α and the through-thickness coordinate θ^3. Derivatives with respect to these coordinates are denoted by $(\cdot)_{,i} = \partial(\cdot)/\partial\theta^i$.

The covariant basis of the mid-surface is represented by $\mathbf{a}_i$

$$\mathbf{a}_\alpha = \frac{\partial \mathbf{r}}{\partial \theta^\alpha}, \quad \mathbf{a}_3 = \mathbf{n} = \frac{\mathbf{a}_1 \times \mathbf{a}_2}{|\mathbf{a}_1 \times \mathbf{a}_2|}, \tag{4}$$

and the first fundamental form is $a_{\alpha\beta} = \mathbf{a}_\alpha \cdot \mathbf{a}_\beta$. The curvature tensor $b_{\alpha\beta}$ is represented by the second fundamental form of surfaces, which can be obtained using the Hessian of the surface $\mathbf{a}_{\alpha,\beta}$ or the derivative of the normal vector $\mathbf{n}_{,\alpha}$

$$b_{\alpha\beta} = \mathbf{n} \cdot \mathbf{a}_{a,b} = -\mathbf{n}_{,\beta} \cdot \mathbf{a}_\alpha. \tag{5}$$

The derivative of the normal vector can be obtained by Weingarten's formula $\mathbf{n}_{,\alpha} = -b_\alpha^\beta \mathbf{a}_\beta$ with $b_\alpha^\beta = a^{\alpha\gamma} b_{\gamma\beta}$ as the mixed curvature tensor [27]. Taking the derivative of Eq. (3), the covariant basis of the shell coordinate system $\mathbf{x}$ can be formulated as follows:

$$\mathbf{g}_\alpha \equiv \mathbf{x}_{,\alpha} = \mathbf{a}_\alpha + \theta^3 \mathbf{n}_{,\alpha}, \quad \mathbf{g}_3 \equiv \mathbf{x}_{,3} = \mathbf{n}. \tag{6}$$

The metric coefficients are constructed by taking the inner-product of these basis vectors, i.e.

$$g_{\alpha\beta} = \mathbf{g}_\alpha \cdot \mathbf{g}_\beta = a_{\alpha\beta} + \theta^3 \left(\mathbf{n}_{,\alpha} \cdot \mathbf{a}_\beta + \mathbf{n}_{,\beta} \cdot \mathbf{a}_\alpha \right) + \left(\theta^3 \right)^2 \mathbf{n}_{,\alpha} \cdot \mathbf{n}_{,\beta} = a_{\alpha\beta} - 2\theta^3 b_{\alpha\beta} + \left(\theta^3 \right)^2 \mathbf{n}_{,\alpha} \cdot \mathbf{n}_{,\beta}, \tag{7}$$

where in the second equality, Eq. (5) is used. Moreover, $g_{\alpha 3} = 0$ and $g_{33} = 1$ [10]. Using the definition of the covariant metric g_{ij}, the contravariant metric g^{ij} and basis vectors $\mathbf{g}^i$ can be found:

$$g^{\alpha\beta} = [g_{\alpha\beta}]^{-1}, \quad \mathbf{g}^\alpha = g^{\alpha\beta} \mathbf{g}_\beta. \tag{8}$$

The third contravariant basis vector $\mathbf{g}_3$ is again the normal vector $\mathbf{n}$ since it has unit-length by construction (see Eq. (4)).

Remark 1. In the isogeometric Kirchhoff-Love shell formulations [10, 12], the last term in Eq. (7) is neglected because of the thin shell assumption, meaning $(\theta^3)^2$ takes small values. However, the co- and contravariant basis vectors ($\mathbf{g}_\alpha$ and $\mathbf{g}^\alpha$, respectively) are used in the mapping of the stretch-based material matrix onto the contravariant undeformed basis (Section 5.3). To enable an accurate comparison of the invariant-based and stretch-based formulation, we do not neglect the $O((\theta^3)^2)$ term, contrary to previous works [12, 15].

2.3. Shell Kinematics

The deformed and undeformed configurations ($\mathbf{x}$ and $\mathring{\mathbf{x}}$, respectively) are related to each other by the mid-plane deformation vector $\mathbf{u}$ by $\mathbf{r} = \mathring{\mathbf{r}} + \mathbf{u}$ and $\mathbf{n} = \mathbf{n}(\mathring{\mathbf{r}} + \mathbf{u})$. However, in both the invariant-based and stretch-based forms that are described in this paper, the deformations are defined using the undeformed and deformed geometries. In continuum mechanics, we define the deformation gradient $\mathbf{F}$ and the deformation tensor $\mathbf{C}$ are defined as [12, 26]:

$$\mathbf{F} = \frac{\mathrm{d}\boldsymbol{x}}{\mathrm{d}\mathring{\boldsymbol{x}}} = \mathbf{g}_i \otimes \mathring{\mathbf{g}}^j, \quad \mathbf{C} = \mathbf{F}^\top \mathbf{F} = \mathbf{g}_i \cdot \mathbf{g}_j \, \mathring{\mathbf{g}}^i \otimes \mathring{\mathbf{g}}^j = g_{ij} \, \mathring{\mathbf{g}}^i \otimes \mathring{\mathbf{g}}^j. \tag{9}$$

Note that the deformation tensor is defined in the contravariant undeformed basis $\mathbf{g}^i \otimes \mathbf{g}^j$. For shells, it is known that $g_{\alpha 3} = g_{3\alpha} = 0$, hence this implies $C_{\alpha 3} = C_{3\alpha} = 0$. Since $g_{33} = 1$, which implies C_{33} to be unity and meaning that the thickness remains constant under deformation. In hyperelastic Kirchhoff-Love shell formulations, the contribution of C_{33} is therefore incorporated by *static condensation* (incompressible materials) or iteratively (compressible materials). Therefore, we denote the deformation tensor $\mathbf{C}$ and its inverse $\bar{\mathbf{C}}$ as denoted as:

$$\mathbf{C} = g_{\alpha\beta} \, \mathring{\mathbf{g}}^\alpha \otimes \mathring{\mathbf{g}}^\beta + C_{33} \mathring{\mathbf{n}} \otimes \mathring{\mathbf{n}}, \tag{10}$$

$$\bar{\mathbf{C}} = g^{\alpha\beta} \, \mathring{\mathbf{g}}_\alpha \otimes \mathring{\mathbf{g}}_\beta + \frac{1}{C_{33}} \mathring{\mathbf{n}} \otimes \mathring{\mathbf{n}}. \tag{11}$$

From Eqs. (10) and (11), it can be observed that the thickness-contribution (index 3) is decoupled from the in-plane contributions (Greek indices α, β). This decoupling is a consequence of the Kirchhoff Hypothesis and therefore is only valid for Kirchhoff-Love shells. As a consequence,

using the definition $\tilde{\mathbf{C}} = g_{\alpha\beta}\mathring{\mathbf{g}}^{\alpha} \otimes \mathring{\mathbf{g}}^{\beta}$, the trace and determinant of $\mathbf{C}$ can be simplified accordingly [24, 25]:

$$\operatorname{tr}\mathbf{C} \equiv \operatorname{tr}\tilde{\mathbf{C}} + C_{33} = g_{\alpha\beta}g^{\alpha\beta} + C_{33}, \tag{12}$$

$$\det\{\mathbf{C}\} = \det\{\mathbf{F}\}^2 \equiv J^2 = \frac{\left|g_{\alpha\beta}\right|}{\left|\mathring{g}_{\alpha\beta}\right|}C_{33} \equiv J_0^2 C_{33} = \lambda_1^2\lambda_2^2\lambda_3^2, \tag{13}$$

where J denotes the *Jacobian determinant* and J_0 is its in-plane counterpart. Furthermore, the tensor invariants of $\mathbf{C}$ simplify to:

$$I_1 := \operatorname{tr}\{\mathbf{C}\} = g_{\alpha\beta}\mathring{g}^{\alpha\beta} + C_{33} = \lambda_1^2 + \lambda_2^2 + \lambda_3^2, \tag{14}$$

$$I_2 := \frac{1}{2}\Big(\operatorname{tr}\{\mathbf{C}\}^2 - \operatorname{tr}\Big\{\mathbf{C}^2\Big\}\Big) = C_{33}g_{\alpha\beta}\mathring{g}^{\alpha\beta} + J_0^2 = \lambda_1^2\lambda_2^2 + \lambda_2^2\lambda_3^2 + \lambda_1^2\lambda_3^2, \tag{15}$$

$$I_3 := \det\{\mathbf{C}\} = \lambda_1^2\lambda_2^2\lambda_3^2, \tag{16}$$

where λ_i denote the *principal stretches* of the shell and their squares λ_i^2 are the eigenvalues of the deformation tensor $\mathbf{C}$. The squares of the eigenvalues are the roots of the characteristic polynomial:

$$(\lambda_i^2)^3 - I_1(\lambda_i^2)^2 + I_2\lambda_i^2 - I_3 = 0. \tag{17}$$

Corresponding eigenvectors are denoted by $\mathbf{v}_i$, which are normalized to have unit-length. The eigenvalue decomposition (or *spectral decomposition*) of the deformation tensor $\mathbf{C}$ can be written as [24, 25]:

$$\mathbf{C} = C_{ij}\mathring{\mathbf{g}}_i \otimes \mathring{\mathbf{g}}_j \equiv \lambda_i^2 \mathbf{v}_i \otimes \mathbf{v}_i. \tag{18}$$

Where the Einstein summation convention is used. Since C_{33} is decoupled by construction, one can immediately see from Eqs. (10) and (18) that $\lambda_3 = \sqrt{C_{33}}$ and $\mathbf{v}_3 = \mathring{\mathbf{n}}$.

For the sake of completeness, we recall the definition of the Green-Lagrange strain tensor $\mathbf{E} = E_{\alpha\beta}\,\mathring{\mathbf{g}}^{\alpha} \otimes \mathring{\mathbf{g}}^{\beta}$ from [10, 12] and its decomposition to membrane and bending contributions ($\boldsymbol{\varepsilon}$ and $\boldsymbol{\kappa}$, respectively):

$$E_{\alpha\beta} = \frac{1}{2}\Big(g_{\alpha\beta} - \mathring{g}_{\alpha\beta}\Big) = \frac{1}{2}\Big((a_{\alpha\beta} - \mathring{a}_{\alpha\beta}) - 2\theta^3\Big(b_{\alpha\beta} - \mathring{b}_{\alpha\beta}\Big)\Big) + \equiv \varepsilon_{\alpha\beta} + \theta_3\kappa_{\alpha\beta}. \tag{19}$$

Remark 2. Following up on Remark 1; the contribution of the $O\Big(\big(\theta^3\big)^2\Big)$ term in Eq. (7) is neglected in the strain tensor and its derivatives. The $O\Big(\big(\theta^3\big)^2\Big)$ term is only included in Eq. (7) to ensure equivalence in comparison of the stretch- and invariant-based formulations.

2.4. Variational Formulation

The shell internal and external equilibrium equations in variational form are derived by the principle of virtual work [10, 12]. The variations of internal and external work are defined as:

$$\delta W(\mathbf{u}, \delta\mathbf{u}) = \delta W^{\text{int}} - \delta W^{\text{ext}} = \int_{\Omega} \mathbf{n} : \delta\boldsymbol{\varepsilon} + \mathbf{m} : \delta\boldsymbol{\kappa}\,\mathrm{d}\Omega - \int_{\Omega} \mathbf{f} \cdot \delta\mathbf{u}\,\mathrm{d}\Omega\,, \tag{20}$$

with $\delta\mathbf{u}$ being the virtual displacement, $\delta\boldsymbol{\varepsilon}$ and $\delta\boldsymbol{\kappa}$ the virtual strain components, Ω the mid-surface and $\mathrm{d}\Omega = \sqrt{\left|\mathring{a}_{\alpha\beta}\right|}\mathrm{d}\theta^1\mathrm{d}\theta^2$ the differential area in the undeformed configuration, mapped

to the integration domain $\Omega^* = [0,1]^2$ using the undeformed mid-plane measure. Furthermore, with slight abuse of notation, the tensors $\mathbf{n} = n^{\alpha\beta}\,\mathring{\mathbf{g}}_\alpha \otimes \mathring{\mathbf{g}}_\beta$ and $\mathbf{m} = m^{\alpha\beta}\,\mathring{\mathbf{g}}_\alpha \otimes \mathring{\mathbf{g}}_\beta$ denote the shell normal force and bending moment tensors, respectively, represented by:

$$n^{\alpha\beta} = \int_{[-t/2,t/2]} S^{\alpha\beta}\,\mathrm{d}\theta^3\,, \quad m^{\alpha\beta} = \int_{[-t/2,t/2]} \theta^3 S^{\alpha\beta}\,\mathrm{d}\theta^3\,. \tag{21}$$

Here, $S^{\alpha\beta}$ denotes the coefficients of the stress tensor following from the constitutive relations that will be derived in Sections 3 and 4 and t stands for the shell thickness. The total differentials of the stress resultants are:

$$\begin{aligned} \mathrm{d}n^{\alpha\beta} &= \int_{[-t/2,t/2]} \mathbb{C}^{\alpha\beta\gamma\delta}\,\mathrm{d}\theta^3\,\mathrm{d}\varepsilon_{\gamma\delta} + \int_{[-t/2,t/2]} \mathbb{C}^{\alpha\beta\gamma\delta}\theta^3\,\mathrm{d}\theta^3\,\mathrm{d}\kappa_{\gamma\delta}\,, \\ \mathrm{d}m^{\alpha\beta} &= \int_{[-t/2,t/2]} \mathbb{C}^{\alpha\beta\gamma\delta}\theta^3\,\mathrm{d}\theta^3\,\mathrm{d}\varepsilon_{\gamma\delta} + \int_{[-t/2,t/2]} \mathbb{C}^{\alpha\beta\gamma\delta}\left(\theta^3\right)^2\,\mathrm{d}\theta^3\,\mathrm{d}\kappa_{\gamma\delta}\,. \end{aligned} \tag{22}$$

Discretizing the equations using known formulations from previous publications [10, 12, 27], the solution $\mathbf{u}$ is represented by a finite sum of weighted basis functions and the tensors $\mathbf{n}$, $\mathbf{m}$, $\boldsymbol{\varepsilon}$ and $\boldsymbol{\kappa}$ are linearized around the weights using Gateaux derivatives. The linearized tensors are denoted by $(\cdot)' = \frac{\partial(\cdot)}{\partial u_r}$ in the following, where u_r are individual weights of the solution vector. Note that $\mathbf{u}'$ denotes the basis functions [12]. Using the discretized system, the residual vector is defined by:

$$R_r = F_r^{\mathrm{int}} - F_r^{\mathrm{ext}} = \int_\Omega \mathbf{n} : \frac{\partial \boldsymbol{\varepsilon}}{\partial u_r} + \mathbf{m} : \frac{\partial \boldsymbol{\kappa}}{\partial u_r}\,\mathrm{d}\Omega - \int_\Omega \mathbf{f} \cdot \frac{\partial \mathbf{u}}{\partial u_r}\,\mathrm{d}\Omega\,, \tag{23}$$

and must be equal to the zero vector for the weights $\mathbf{u}$ corresponding to the exact solution. To solve the residual equation $\mathbf{R} = \mathbf{0}$, another linearization is performed, yielding the Jacobian matrix or *tangential stiffness matrix* K:

$$K_{rs} = K_{rs}^{\mathrm{int}} - K_{rs}^{\mathrm{ext}} = \int_\Omega \frac{\partial \mathbf{n}}{\partial u_s} : \frac{\partial \boldsymbol{\varepsilon}}{\partial u_r} + \mathbf{n} : \frac{\partial^2 \boldsymbol{\varepsilon}}{\partial u_r \partial u_s} + \frac{\partial \mathbf{m}}{\partial u_s} : \frac{\partial \boldsymbol{\kappa}}{\partial u_r} + \mathbf{m} : \frac{\partial^2 \boldsymbol{\kappa}}{\partial u_r \partial u_s}\,\mathrm{d}\Omega - \int_\Omega \frac{\partial \mathbf{f}}{\partial u_s} \cdot \frac{\partial \mathbf{u}}{\partial u_r}\,\mathrm{d}\Omega\,. \tag{24}$$

Note that the matrix contains a contribution for the external load depending on the solution vector ($\mathbf{f}(\mathbf{u})$). For instance, follower-pressures are defined by $\mathbf{f}(\mathbf{u}) = p\mathbf{n}(\mathbf{u})$, where $\mathbf{n}$ is the surface normal. In order to solve for nonlinear equation, Newton iterations are performed for solution $\mathbf{u}$ and increment $\Delta\mathbf{u}$ by solving

$$K\Delta\mathbf{u} = -\mathbf{R}. \tag{25}$$

3. Invariant-Based Constitutive Relations

Adopting an invariant-based formulation [12], the constitutive relations for hyperelastic shells are derived and illustrated for the Mooney-Rivlin material model. That is, the constitutive laws are derived using derivatives of the strain energy density function $\Psi(\mathbf{C})$ with respect to the components C_{ij} of the deformation tensor $\mathbf{C}$. The aim of this section is to keep the paper self-contained and to show the relation between the state-of-the-art [12] and the novel formulations that will be presented in Section 4.

The section is structured as follows: Section 3.1 provides general formulations and background that are valid for both compressible and incompressible material formulations. Thereafter, Section 3.2 and Section 3.3 provide the derivations for incompressible and compressible material models, respectively, in the invariant-based formulations. As mentioned before, these formulations are based on [12].

3.1. General Relations

Firstly, the second Piola-Kirchhoff stress tensor $\mathbf{S} = S^{ij}\,\mathring{\mathbf{g}}_i \otimes \mathring{\mathbf{g}}_j$ and the (tangent) material tensor $\mathbb{C} = \mathbb{C}^{ijkl}\,\mathring{\mathbf{g}}_i \otimes \mathring{\mathbf{g}}_j \otimes \mathring{\mathbf{g}}_k \otimes \mathring{\mathbf{g}}_l$ are defined by the following well-established relations [12, 24–26]:

$$S^{ij} = \frac{\partial \Psi}{\partial E_{ij}} = 2\frac{\partial \Psi}{\partial C_{ij}}, \quad \mathbb{C}^{ijkl} = \frac{\partial^2 \Psi}{\partial E_{ij}\partial E_{kl}} = 4\frac{\partial^2 \Psi}{\partial C_{ij}\partial C_{kl}}. \tag{26}$$

These equations are valid for 3D continua and hence need to be modified for the shell equations to incorporate the through-thickness stress components. Reading Eq. (10), $C_{\alpha\beta} = g_{\alpha\beta}$ but $C_{33} \neq g_{33} = 1$ to avoid violation of the plane stress condition. To correctly incorporate the plane-stress condition ($S_{33} = 0$), the material tensor $\mathbb{C}$ is modified using static condensation, which implies that the material tensor $\hat{\mathbb{C}}$ corrected for plane-stress is defined by [12]:

$$\hat{\mathbb{C}}^{\alpha\beta\gamma\delta} = \mathbb{C}^{\alpha\beta\delta\gamma} - \frac{\mathbb{C}^{\alpha\beta 33}\mathbb{C}^{33\delta\gamma}}{\mathbb{C}^{3333}}. \tag{27}$$

For incompressible materials, this term is derived analytically using the incompressibility condition ($J = 1$) whereas for compressible materials, it is corrected iteratively.

3.2. Incompressible Material Models

For incompressible materials, the incompressibility condition ($J = 1$) is enforced using a Lagrange multiplier p in the strain energy density function [12, 24]:

$$\Psi(\mathbf{C}) = \Psi_{el}(\mathbf{C}) - p(J-1), \tag{28}$$

where Ψ_{el} is the original strain energy density function. Using Eq. (28), Eq. (26) reduces to [12]:

$$S^{ij} = 2\frac{\partial \Psi_{el}}{\partial C_{ij}} - 2\frac{\partial p}{\partial C_{ij}}(J-1) - 2p\frac{\partial J}{\partial C_{ij}}, \tag{29}$$

$$\mathbb{C}^{ijkl} = 4\frac{\partial^2 \Psi_{el}}{\partial C_{ij}\partial C_{kl}} - 4\frac{\partial^2 p}{\partial C_{ij}\partial C_{kl}}(J-1) - 4\frac{\partial p}{\partial C_{ij}}\frac{\partial J}{\partial C_{kl}} - 4\frac{\partial J}{\partial C_{ij}}\frac{\partial p}{\partial C_{kl}} - 4p\frac{\partial^2 J}{\partial C_{ij}\partial C_{kl}}. \tag{30}$$

The plane stress condition ($S_{33} = 0$) together with the incompressibility condition ($J = 1$) lead to the expression for the Lagrange multiplier p, from which its derivative with respect to C_{ij} can easily be obtained [12]:

$$p = 2\frac{\partial \Psi_{el}}{\partial C_{33}}C_{33}, \tag{31}$$

$$\frac{\partial p}{\partial C_{ij}} = 2\left(\frac{\partial^2 \Psi_{el}}{\partial C_{33}\partial C_{ij}}C_{33} + \frac{\partial \Psi_{el}}{\partial C_{33}}\delta^{i3}\delta^{j3}\right) \tag{32}$$

Substituting the derivatives of the Jacobian determinant J (see Eqs. (A.2) and (A.4) in Appendix A), Eqs. (29) and (30) reduce to the following equations, which are valid for incompressible materials in general with $S_{33} = 0$ enforced [12]:

$$S^{ij} = 2\frac{\partial \Psi_{el}}{\partial C_{ij}} - 2\frac{\partial \Psi_{el}}{\partial C_{33}} C_{33} \bar{C}^{ij}, \tag{33}$$

$$\begin{aligned}\mathbb{C}^{ijkl} = {} & 4\frac{\partial^2 \Psi_{el}}{\partial C_{ij} \partial C_{kl}} - 4\left(\frac{\partial^2 \Psi_{el}}{\partial C_{33} \partial C_{ij}} C_{33} + \frac{\partial \Psi_{el}}{\partial C_{33}} \delta^{i3}\delta^{j3}\right)\bar{C}^{kl} - 4\bar{C}^{ij}\left(\frac{\partial^2 \Psi_{el}}{\partial C_{33} \partial C_{kl}} C_{33} + \frac{\partial \Psi_{el}}{\partial C_{33}} \delta^{k3}\delta^{l3}\right) \\ & - 2\frac{\partial \Psi_{el}}{\partial C_{33}} C_{33}\left(\bar{C}^{ij}\bar{C}^{kl} - \bar{C}^{ik}\bar{C}^{jl} - \bar{C}^{il}\bar{C}^{jk}\right).\end{aligned} \tag{34}$$

For a shell, note that only the in-plane components $S^{\alpha\beta}$ and $\mathbb{C}^{\alpha\beta\gamma\delta}$ are only considered and that $C^{-1}_{\alpha\beta} = \bar{C}^{\alpha\beta} = g^{\alpha\beta}$, $C_{33} = J_0^{-2}$. The stress-tensor and the material tensor for incompressible Kirchhoff-Love shells become, by substituting Eqs. (10) and (11):

$$S^{\alpha\beta} = 2\frac{\partial \Psi_{el}}{\partial C_{\alpha\beta}} - 2\frac{\partial \Psi_{el}}{\partial C_{33}} J_0^{-2} g^{\alpha\beta}, \tag{35}$$

$$\hat{\mathbb{C}}^{\alpha\beta\gamma\delta} = 4\frac{\partial^2 \Psi_{el}}{\partial C_{\alpha\beta} \partial C_{\gamma\delta}} + 4J_0^{-4} g^{\alpha\beta} g^{\gamma\delta} \frac{\partial^2 \Psi_{el}}{\partial C_{33}^2} - 4\frac{\partial^2 \Psi_{el}}{\partial C_{33} \partial C_{\alpha\beta}} J_0^{-2} g^{\gamma\delta} \tag{36}$$

$$- 4g^{\alpha\beta} J_0^{-2} \frac{\partial^2 \Psi_{el}}{\partial C_{33} \partial C_{\gamma\delta}} + 2\frac{\partial \Psi_{el}}{\partial C_{33}} J_0^{-2}\left(2g^{\alpha\beta} g^{\gamma\delta} + g^{\alpha\gamma} g^{\beta\delta} + g^{\alpha\delta} g^{\beta\gamma}\right). \tag{37}$$

Example 1 (*Incompressible Mooney-Rivlin Model*)**.** The strain energy density function of the incompressible Mooney-Rivlin material model is defined as follows [28, 29]:

$$\Psi_{el} = \frac{c_1}{2}(I_1 - 3) + \frac{c_2}{2}(I_2 - 3), \tag{38}$$

where c_1 and c_2 are the material parameters such that the Lamé parameter μ satisfies $\mu = c_1 + c_2$. Using the derivatives of the invariants I_1 and I_2 and the Jacobian determinant J with respect to C_{ij}, the derivatives of Ψ can be found using the identities in Appendix A (see Eqs. (A.2) and (A.4) to (A.9)):

$$\frac{\partial \Psi}{\partial C_{\alpha\beta}} = \frac{c_1}{2}\mathring{g}^{\alpha\beta} + \frac{c_2}{2}\left(C_{33}\mathring{g}^{\alpha\beta} + J_0^2 g^{\alpha\beta}\right), \qquad \frac{\partial \Psi}{\partial C_{33}} = \frac{c_1}{2} + \frac{c_2}{2}\operatorname{tr}\tilde{\mathbf{C}}, \tag{39}$$

$$\frac{\partial^2 \Psi}{\partial C_{\alpha\beta} \partial C_{\gamma\delta}} = \frac{c_2}{2}\left(J_0^2 g^{\alpha\beta} g^{\gamma\delta} - \frac{1}{2}J_0^2\left(g^{\alpha\gamma} g^{\beta\delta} + g^{\alpha\delta} g^{\beta\gamma}\right)\right), \qquad \frac{\partial^2 \Psi}{\partial C_{33} \partial C_{\alpha\beta}} = \frac{\partial^2 \Psi}{\partial C_{\alpha\beta} \partial C_{33}} = \frac{c_2}{2}\mathring{g}^{\alpha\beta}, \tag{40}$$

and all other derivatives are equal to zero. As a consequence, Eqs. (35) and (37) reduce to:

$$S^{\alpha\beta} = c_1\left(\mathring{g}^{\alpha\beta} - J_0^{-2} g^{\alpha\beta}\right) + c_2\left(J_0^{-2}\mathring{g}^{\alpha\beta} + J_0^2 g^{\alpha\beta} - \operatorname{tr}\tilde{\mathbf{C}} J_0^{-2} g^{\alpha\beta}\right), \tag{41}$$

$$\mathbb{C}^{\alpha\beta\gamma\delta} = \left(c_1 + c_2 \operatorname{tr}\tilde{\mathbf{C}}\right)\left(2g^{\alpha\beta} g^{\gamma\delta} + g^{\alpha\gamma} g^{\beta\delta} + g^{\alpha\delta} g^{\beta\gamma}\right) - 2c_2 J_0^{-2}\left(\mathring{g}^{\alpha\beta} g^{\gamma\delta} + g^{\alpha\beta}\mathring{g}^{\gamma\delta}\right) \tag{42}$$

$$+ c_2 J_0^2\left(2g^{\alpha\beta} g^{\gamma\delta} - g^{\alpha\gamma} g^{\beta\delta} - g^{\alpha\delta} g^{\beta\gamma}\right). \tag{43}$$

Note that for $c_1 = \mu$ and $c_2 = 0$, this model reduces to the incompressible Neo-Hookean material model (see Eq. (96)) [12].

3.3. Compressible Material Models

For compressible models, the Jacobian determinant J is not necessarily equal to 1. As a consequence, the deformation gradient $\mathbf{F}$ and deformation tensor $\mathbf{C}$ are modified such that $\mathbf{F}$ and $\mathbf{C}$ are a multiplicative decomposition of a volume-changing (*dilational*) part depending on J and a volume preserving (*distortional*) part depending on the modified deformation gradient and deformation tensors, $\dot{\mathbf{C}}$ and $\dot{\mathbf{F}}$, respectively [30]:

$$\dot{\mathbf{F}} = J^{-\frac{1}{3}}\mathbf{F}, \quad \dot{\mathbf{C}} = J^{-\frac{2}{3}}\mathbf{C}. \tag{44}$$

The modified deformation gradient and deformation tensor have determinants which are equal to 1 (corresponding to volume preservation), meaning:

$$\det\left\{\dot{\mathbf{F}}\right\} = \dot{\lambda}_1\dot{\lambda}_2\dot{\lambda}_3 = 1, \quad \det\left\{\dot{\mathbf{C}}\right\} = 1, \tag{45}$$

where the modified principal stretches $\dot{\lambda}_i$ are defined as:

$$\dot{\lambda}_i = J^{-\frac{1}{3}}\lambda_i. \tag{46}$$

As a consequence, the invariants of the modified deformation tensor $\dot{\mathbf{C}}$ become:

$$\dot{I}_1 = J^{-2/3}I_1, \quad \dot{I}_2 = J^{-4/3}I_2, \quad \dot{I}_3 = 1, \tag{47}$$

with I_i the invariants of the deformation tensor $\mathbf{C}$. With $\dot{\mathbf{F}}, \dot{\mathbf{C}}$ and $\dot{I}_k$ defined above, the strain energy density function $\Psi(\mathbf{C})$ for a compressible material can be described in a decoupled form, separating the response in a isochoric (or distortional) elastic part $\Psi_{\text{iso}}(\dot{\mathbf{C}})$ and an volumetric (or dilational) elastic part $\Psi_{\text{vol}}(J)$ [24, 25, 30]:

$$\Psi(\mathbf{C}) = \Psi_{\text{iso}}(\dot{\mathbf{C}}) + \Psi_{\text{vol}}(J). \tag{48}$$

The volumetric elastic part Ψ_{vol} is required to be strictly convex and equal to zero if and only if $J = 1$ and $\dot{\mathbf{C}} = \mathbf{I}$ [24].

For compressible materials, the plane stress condition is incorporated by iteratively solving $S_{33} = 0$ for C_{33} using Newton linearizations [12, 31]:

$$S^{33} + \frac{1}{2}\Delta\mathbb{C}_{3333}\Delta C_{33} = 0. \tag{49}$$

where C_{33} is incrementally updated by $C_{33}^{(n+1)} = C_{33}^{(n)} + \Delta C_{33}^{(n)}$ with the increment on iteration n:

$$\Delta C_{33}^{(n)} = -2\frac{S_{(n)}^{33}}{\mathbb{C}_{(n)}^{3333}}. \tag{50}$$

In each iteration, the updated stress tensor $\mathbf{S}$ and material tensor $\mathbb{C}$ can be computed and iterations are continued until the plane stress condition is satisfied within a certain tolerance, i.e. $\left|S^{33}\right| < \text{tol}$. When converged, static condensation can be performed for the material tensor using Eq. (27). Rather than using $C_{33}^{(0)} = 0$ [12], $C_{33}^{(0)} = J_0^{-2}$ is used for incompressible materials, although the difference for the two approaches is negligible.

Example 2 (*Compressible Mooney-Rivlin Model*)**.** The strain energy density function of the Mooney-Rivlin material model is defined as:[24]

$$\Psi = \Psi_{\text{vol}}(\dot{\mathbf{C}}) + \Psi_{\text{iso}}(J) = \frac{c_1}{2}\Big(J^{-\frac{2}{3}} I_1 - 3\Big) + \frac{c_2}{2}\Big(J^{-\frac{4}{3}} I_2 - 3\Big) + K\mathcal{G}(J), \tag{51}$$

where c_1 and c_2 are the material parameters such that the Lamé parameter μ satisfies $\mu = c_1 + c_2$. The bulk modulus of the material is $K = 2\mu(1+\nu)/(3-6\nu)$ and the function contribution $K\mathcal{G}(J)$ is the volumetric contribution function of which $\mathcal{G}$ is defined as [32]:

$$\mathcal{G}(J) = \beta^{-2}\Big(\beta \log(J) + J^{-\beta} - 1\Big). \tag{52}$$

The parameter β is an empirical coefficient and a value of -2 can be adopted [33]. Note that for the volumetric strain energy density function Ψ_{vol} other functions can be selected as well [34]. Using the derivatives of the invariants I_1 and I_2 and the Jacobian determinant J with respect to C_{ij}, the derivatives of Ψ can be obtained:

$$\frac{\partial \Psi}{\partial C_{ij}} = \frac{c_1}{2}\left(J^{-\frac{2}{3}}\frac{\partial I_1}{\partial C_{ij}} - \frac{1}{3}J^{-\frac{2}{3}} I_1 \bar{C}^{ij}\right) + \frac{c_2}{2}\left(J^{-\frac{4}{3}}\frac{\partial I_2}{\partial C_{ij}} - \frac{2}{3}J^{-\frac{4}{3}} I_2 \bar{C}^{ij}\right) + \frac{K}{2\beta}\Big(1 - J^{-\beta}\Big)\bar{C}^{ij}, \tag{53}$$

$$\begin{aligned}\frac{\partial^2 \Psi}{\partial C_{ij}\partial C_{kl}} &= \frac{1}{9}\frac{c_1}{2}J^{-\frac{2}{3}}\left(I_1 \bar{C}^{ij}\bar{C}^{kl} - 3\frac{\partial I_1}{\partial C_{ij}}\bar{C}^{kl} - 3\frac{\partial I_1}{\partial C_{kl}}\bar{C}^{ij} - 3I_1\frac{\partial \bar{C}_{ij}}{\partial C_{kl}} + 9\frac{\partial^2 I_1}{\partial C_{ij}\partial C_{kl}}\right) \\ &+ \frac{1}{9}\frac{c_2}{2}J^{-\frac{4}{3}}\left(4I_1 \bar{C}^{ij}\bar{C}^{kl} - 6\frac{\partial I_1}{\partial C_{ij}}\bar{C}^{kl} - 6\frac{\partial I_1}{\partial C_{kl}}\bar{C}^{ij} - 6I_1\frac{\partial \bar{C}_{ij}}{\partial C_{kl}} + 9\frac{\partial^2 I_1}{\partial C_{ij}\partial C_{kl}}\right) \\ &+ \frac{K}{4\beta}\left(\beta J^{-\beta}\bar{C}^{ij}\bar{C}^{kl} + 2\Big(1 - J^{-\beta}\Big)\frac{\partial \bar{C}^{ij}}{\partial C_{kl}}\right),\end{aligned} \tag{54}$$

where for the sake of brevity, reference is made to Eqs. (A.5) to (A.9) in Appendix A for the derivatives of the invariants and to Eq. (2) for the derivative of the inverse of the deformation tensor. Note that from Eq. (A.6) it follows that the second derivative of I_1 is equal to zero. The other derivatives of the invariants and the derivative of the inverse of the deformation tensor are not substituted for conciseness. Substituting Eqs. (53) and (54) into Eq. (26) yields expressions for the stress and material tensors:

$$S^{\alpha\beta} = c_1 J^{-\frac{2}{3}}\left(\frac{\partial I_1}{\partial C_{ij}} - \frac{1}{3}I_1 \bar{C}^{ij}\right) + c_2 J^{-\frac{4}{3}}\left(\frac{\partial I_2}{\partial C_{ij}} - \frac{2}{3}I_2 \bar{C}^{ij}\right) + \frac{K}{\beta}\Big(1 - J^{-\beta}\Big)\bar{C}^{ij}, \tag{55}$$

$$\begin{aligned}\mathbb{C}^{ijkl} &= \frac{1}{9}c_1 J^{-\frac{2}{3}}\left(2I_1 \bar{C}^{ij}\bar{C}^{kl} - 6\frac{\partial I_1}{\partial C_{ij}}\bar{C}^{kl} - 6\frac{\partial I_1}{\partial C_{kl}}\bar{C}^{ij} - 6I_1\frac{\partial \bar{C}^{ij}}{\partial C_{kl}}\right) \\ &+ \frac{1}{9}c_2 J^{-\frac{4}{3}}\left(8I_2 \bar{C}^{ij}\bar{C}^{kl} - 12\frac{\partial I_2}{\partial C_{ij}}\bar{C}^{kl} - 12\frac{\partial I_2}{\partial C_{kl}}\bar{C}^{ij} - 12I_2\frac{\partial \bar{C}^{ij}}{\partial C_{kl}} + 18\frac{\partial^2 I_2}{\partial C_{ij}\partial C_{kl}}\right) \\ &+ \frac{K}{\beta}\left(\beta J^{-\beta}\bar{C}^{ij}\bar{C}^{kl} + 2\Big(1 - J^{-\beta}\Big)\frac{\partial \bar{C}^{ij}}{\partial C_{kl}}\right).\end{aligned} \tag{56}$$

Again, for $c_1 = \mu$ and $c_2 = 0$, this material model reduces to the Neo-Hookean model (see Eq. (95)) [12].

4. Stretch-Based Constitutive Relations

Invariant-based (in)compressible material model formulations have been obtained for the strain energy density functions $\Psi(\mathbf{C})$ in Section 3 based on [12]. However, when experimental

material data fitting is involved a formulation in terms of stretches (i.e. in terms of the eigenvalues of $\mathbf{C}$, $\Psi(\boldsymbol{\lambda}$ with $\boldsymbol{\lambda} = (\lambda_1, \lambda_2, \lambda_3))$ might be preferred, meaning the invariant-based formulations (Section 3) are not directly applicable. Therefore, this section provides the main contribution of this paper: the generalized formulations for the implementation of stretch-based material models in the isogeometric Kirchhoff-Love shell model.

The section is structured as follows: Section 4.1 provides the basics for the derivation of the stretch-based constitutive relations. Thereafter, Section 4.2 and Section 4.3 provide the derivations for incompressible and compressible material models, respectively, in the stretch-based formulations. These formulations are the novelty of the present paper.

4.1. General Relations

Assuming $\Psi(\boldsymbol{\lambda})$, relations for the stress and material tensor will be derived in terms of the (normalized) eigenvector bases (Eq. (18)):

$$\mathbf{S} = S^i \, \mathbf{v}_i \otimes \mathbf{v}_i, \quad \mathbb{C} = \mathbb{C}^{ijkl} \, \mathbf{v}_i \otimes \mathbf{v}_j \otimes \mathbf{v}_k \otimes \mathbf{v}_l. \tag{57}$$

When $\mathbf{S}$ and $\mathbb{C}$ are known, a transformation to the bases $\mathring{\mathbf{g}}_i \otimes \mathring{\mathbf{g}}_j$ and $\mathring{\mathbf{g}}_i \otimes \mathring{\mathbf{g}}_j \otimes \mathring{\mathbf{g}}_k \otimes \mathring{\mathbf{g}}_l$ for the stress and material tensors, respectively. This will be discussed in Section 5.3.

The derivative of any scalar function with respect to the deformation tensor $\mathbf{C}$ can be written as a derivative with respect to the stretch by applying the chain rule [24]:

$$\frac{\partial(\cdot)}{\partial \mathbf{C}} = \frac{\partial(\cdot)}{\partial \lambda_i^2} \frac{\partial \lambda_i^2}{\partial \mathbf{C}} = \frac{\partial(\cdot)}{\partial \lambda_i^2} \mathbf{v}_i \otimes \mathbf{v}_i = \frac{1}{2\lambda_i} \frac{\partial(\cdot)}{\partial \lambda_i} \mathbf{v}_i \otimes \mathbf{v}_i. \tag{58}$$

Consequently, the second derivatives are:

$$\frac{\partial^2(\cdot)}{\partial \mathbf{C} \partial \mathbf{C}} = \frac{\partial}{\partial \mathbf{C}} \left(\frac{1}{2\lambda_i} \frac{\partial(\cdot)}{\partial \lambda_i} \mathbf{v}_i \otimes \mathbf{v}_i \right) = \frac{1}{4\lambda_i \lambda_j} \frac{\partial^2(\cdot)}{\partial \lambda_i \partial \lambda_i} \mathbf{v}_i \otimes \mathbf{v}_i \otimes \mathbf{v}_j \otimes \mathbf{v}_j. \tag{59}$$

From this, it follows that:

$$\mathbf{S} = 2 \frac{\partial \Psi}{\partial \mathbf{C}} = \frac{1}{\lambda_i} \frac{\partial \Psi}{\partial \lambda_i} \mathbf{v}_i \otimes \mathbf{v}_i \equiv S_i \mathbf{v}_i \otimes \mathbf{v}_i. \tag{60}$$

Furthermore, it can also be shown that for the material tensor, the following holds [5, 6, 8, 24, 35]:

$$\mathbb{C}^{ijkl} = \frac{1}{\lambda_k} \frac{\partial S_i}{\partial \lambda_k} \delta_i^j \delta_k^l + \frac{S_j - S_i}{\lambda_j^2 - \lambda_i^2} (\delta_i^k \delta_j^l + \delta_i^l \delta_j^k)(1 - \delta_i^j). \tag{61}$$

The first part of $\mathbb{C}^{ijkl}$ represents the normal components (diagonal elements) and the second part denotes the shear components (off-diagonal elements). In the formulation of the invariant-based counterpart of this equation (Eq. (26)) these parts are not explicitly visible, since the spectral form by definition uses the principal directions of the deformation tensor, whereas shear and normal contributions are mixed in the curvilinear form of the material tensor. Note that for the second part of this equation, the case $\lambda_i = \lambda_j$ results in an undefined result. Hence, using L'Hopital's rule, this limit case can be identified:

$$\lim_{\lambda_j \to \lambda_i} \frac{S_j - S_i}{\lambda_j^2 - \lambda_i^2} = \lim_{\lambda_j \to \lambda_i} \frac{\frac{\partial S_j}{\partial \lambda_j} - \frac{\partial S_i}{\partial \lambda_j}}{2\lambda_j} = \frac{1}{2\lambda_i} \left(\frac{\partial S_j}{\partial \lambda_j} - \frac{\partial S_i}{\partial \lambda_j} \right). \tag{62}$$

Similar to the derivations in terms of the components (see Section 3) static condensation is also applied to enforce plane-stress. For incompressible material models, the stretch-based static condensation term will be derived. For compressible models, static condensation will be performed iteratively in spectral form and afterwards it will be transformed to the covariant undeformed basis. Since $J = \lambda_1\lambda_2\lambda_3$, the derivatives of J are:

$$\frac{\partial J}{\partial \lambda_i} = \frac{J}{\lambda_i}, \quad \frac{\partial^2 J}{\partial \lambda_j \partial \lambda_j} = (1 - \delta_i^j)\frac{J}{\lambda_i \lambda_j}. \tag{63}$$

4.2. Incompressible Material Models

Similar to the invariant-based formulation (Section 3.2), the incompressibility condition $J = 1$ is imposed using the Lagrange multiplier p in the strain energy density function for incompressible materials, i.e.

$$\Psi(\lambda_i) = \Psi_{el}(\lambda_i) - p(J - 1). \tag{64}$$

Using Eq. (60), the stress tensor becomes:

$$S_i = \frac{1}{\lambda_i}\left(\frac{\partial \Psi_{el}}{\partial \lambda_i} - \frac{\partial p}{\partial \lambda_i}(J - 1) - p\frac{\partial J}{\partial \lambda_i}\right). \tag{65}$$

Comparing S_i with the invariant-based stress tensor in Eq. (29) shows that all components can easily be obtained using Eq. (58). To comply with the plane-stress condition $S^{33} = 0$, the equation to be solved for p using $J = 1$ denotes:

$$\frac{1}{\lambda_3}\left(\frac{\partial \Psi_{el}}{\partial \lambda_3} - p\frac{\partial J}{\partial \lambda_3}\right) = 0, \tag{66}$$

which implies, using the derivative of J from Eq. (A.13):

$$p = \left(\frac{\partial J}{\partial \lambda_3}\right)^{-1}\frac{\partial \Psi_{el}}{\partial \lambda_3} = \lambda_3\frac{\partial \Psi_{el}}{\partial \lambda_3}. \tag{67}$$

It can easily be shown that Eq. (67) is similar to the expression of p in the invariant-based form (Eq. (31)) using Eq. (59) and using $\lambda_3^2 = C_{33}$. The derivative of the stress tensor with respect to the stretch is required to find the material tensor, as observed in Eq. (61). From Eq. (65) it follows that:

$$\begin{aligned}\frac{\partial S_i}{\partial \lambda_j} &= \frac{\partial}{\partial \lambda_j}\left(\frac{1}{\lambda_i}\frac{\partial \Psi}{\partial \lambda_i}\right) = \frac{1}{\lambda_i}\frac{\partial^2 \Psi}{\partial \lambda_i \partial \lambda_j} - \delta_i^j\frac{1}{\lambda_i^2}\frac{\partial \Psi}{\partial \lambda_i} \\ &= \frac{1}{\lambda_i}\left(\frac{\partial^2 \Psi_{el}}{\partial \lambda_i \partial \lambda_j} - \frac{\partial p}{\partial \lambda_i}\frac{\partial J}{\partial \lambda_j} - \frac{\partial p}{\partial \lambda_j}\frac{\partial J}{\partial \lambda_i} - p\frac{\partial^2 J}{\partial \lambda_i \partial \lambda_j} - \delta_i^j\frac{1}{\lambda_i}\left(\frac{\partial \Psi_{el}}{\partial \lambda_i} - p\frac{\partial J}{\partial \lambda_i}\right)\right),\end{aligned} \tag{68}$$

where the incompressibility condition ($J = 1$) is used again. Note that the Kronecker delta δ_i^j covers the case when $i = j$. The derivative of p follows from Eq. (67) and yields:

$$\frac{\partial p}{\partial \lambda_i} = \lambda_3\frac{\partial^2 \Psi_{el}}{\partial \lambda_3 \partial \lambda_i} + \delta_i^3\frac{\partial \Psi_{el}}{\partial \lambda_3}. \tag{69}$$

Again, this result can be compared to its invariant-based counterpart in Eq. (32) and using Eqs. (58) and (59) it can be observed that these equations are similar. Substituting Eqs. (63), (67) and (69) and $J = 1$ into Eqs. (65) and (68) then provides:

$$S_i = \frac{1}{\lambda_i}\left(\frac{\partial \Psi_{el}}{\partial \lambda_i} - \frac{\lambda_3}{\lambda_i}\frac{\partial \Psi_{el}}{\partial \lambda_3}\right), \tag{70}$$

$$\begin{aligned}\frac{\partial S_i}{\partial \lambda_j} = \frac{1}{\lambda_i}\Bigg[&\frac{\partial^2 \Psi_{el}}{\partial \lambda_i \partial \lambda_j} - \frac{1}{\lambda_j}\left(\lambda_3 \frac{\partial^2 \Psi_{el}}{\partial \lambda_3 \partial \lambda_i} + \delta_i^3 \frac{\partial \Psi_{el}}{\partial \lambda_3}\right) - \frac{1}{\lambda_i}\left(\lambda_3 \frac{\partial^2 \Psi_{el}}{\partial \lambda_3 \partial \lambda_j} + \delta_j^3 \frac{\partial \Psi_{el}}{\partial \lambda_3}\right) \\ &- \lambda_3 \frac{\partial \Psi_{el}}{\partial \lambda_3}\frac{(1-\delta_i^j)}{\lambda_i \lambda_j} - \delta_i^j \frac{1}{\lambda_i}\left(\frac{\partial \Psi_{el}}{\partial \lambda_i} - \frac{1}{\lambda_i}\lambda_3 \frac{\partial \Psi_{el}}{\partial \lambda_3}\right)\Bigg].\end{aligned} \tag{71}$$

Comparison with the invariant-based formulation shows that λ_i^{-1} in front of the second term in Eq. (70) translates to $\bar{C}^{ij}$ in Eq. (34). Using these identities, the material tensor can be derived from Eq. (61). For the static condensation term, reference is made to Eq. (27), hence the components $\mathbb{C}^{\alpha\beta 33}$, $\mathbb{C}^{33\alpha\beta}$ and $\mathbb{C}^{3333}$ need to be evaluated. From Eq. (61) it follows that:

$$\mathbb{C}^{\alpha\beta 33} = \frac{1}{\lambda_3}\frac{\partial S_{\alpha\alpha}}{\partial \lambda_3}\delta_\alpha^\beta = -\frac{1}{\lambda_3 \lambda_\alpha^2}\left[\lambda_3 \frac{\partial^2 \Psi_{el}}{\partial \lambda_3^2} + 2\frac{\partial \Psi_{el}}{\partial \lambda_3}\right]\delta_\alpha^\beta, \tag{72}$$

$$\mathbb{C}^{33\gamma\delta} = \frac{1}{\lambda_\gamma}\frac{\partial S_{33}}{\partial \lambda_\gamma}\delta_\gamma^\delta = -\frac{1}{\lambda_3 \lambda_\gamma^2}\left[\lambda_3 \frac{\partial^2 \Psi_{el}}{\partial \lambda_3^2} + 2\frac{\partial \Psi_{el}}{\partial \lambda_3}\right]\delta_\gamma^\delta, \tag{73}$$

$$\mathbb{C}^{3333} = \frac{1}{\lambda_3}\frac{\partial S_{33}}{\partial \lambda_3} = -\frac{1}{\lambda_3^3}\left[\lambda_3 \frac{\partial^2 \Psi_{el}}{\partial \lambda_3^2} + 2\frac{\partial \Psi_{el}}{\partial \lambda_3}\right], \tag{74}$$

such that the static condensation term becomes:

$$\frac{\mathbb{C}^{\alpha\beta 33}\mathbb{C}^{33\gamma\delta}}{\mathbb{C}^{3333}} = -\frac{\frac{1}{\lambda_3^2 \lambda_\alpha^2 \lambda_\gamma^2}\left[\lambda_3 \frac{\partial^2 \Psi_{el}}{\partial \lambda_3^2} + 2\frac{\partial \Psi_{el}}{\partial \lambda_3}\right]^2}{\frac{1}{\lambda_3^3}\left[\lambda_3 \frac{\partial^2 \Psi_{el}}{\partial \lambda_3^2} + 2\frac{\partial \Psi_{el}}{\partial \lambda_3}\right]}\delta_\alpha^\beta \delta_\gamma^\delta \tag{75}$$

$$= -\frac{1}{\lambda_\alpha^2 \lambda_\gamma^2}\left[\lambda_3 \frac{\partial^2 \Psi_{el}}{\partial \lambda_3^2} + 2\frac{\partial \Psi_{el}}{\partial \lambda_3}\right]\delta_\alpha^\beta \delta_\gamma^\delta. \tag{76}$$

Using this result, the in-plane incompressible material tensor can be evaluated as:

$$\mathbb{C}^{\alpha\beta\gamma\delta} = \frac{1}{\lambda_\gamma}\frac{\partial S^{\alpha\alpha}}{\partial \lambda_\gamma}\delta_\alpha^\beta \delta_\gamma^\delta + \frac{S^{\beta\beta} - S^{\alpha\alpha}}{\lambda_\beta^2 - \lambda_\alpha^2}(\delta_\alpha^\gamma \delta_\beta^\delta + \delta_\alpha^\delta \delta_\beta^\gamma)(1-\delta_i^j) - \frac{1}{\lambda_\alpha^2 \lambda_\gamma^2}\left[\lambda_3 \frac{\partial^2 \Psi_{el}}{\partial \lambda_3^2} + 2\frac{\partial \Psi_{el}}{\partial \lambda_3}\right]\delta_\alpha^\beta \delta_\gamma^\delta, \tag{77}$$

where the second term needs to be replaced by Eq. (62) if $\lambda_\alpha = \lambda_\beta$.

Example 3 (*Incompressible Ogden Material Model*)**.** The (incompressible) Ogden material model is an example of a (class of) material model(s) that is expressed in terms of stretches. The strain energy density function reads [24, 25, 32]:

$$\Psi = \sum_{p=1}^{N}\frac{\mu_p}{\alpha_p}\left(\lambda_1^{\alpha_p} + \lambda_2^{\alpha_p} + \lambda_3^{\alpha_p} - 3\right) = \sum_{q=1}^{3}\left(\sum_{p=1}^{N}\frac{\mu_p}{\alpha_p}(\lambda_q^{\alpha_p} - 1)\right) = \sum_{q=1}^{3}\omega(\lambda_q). \tag{78}$$

The last equality signs show that the function can be written as a sum of three separate functions $\omega(\lambda_i)$ depending on different stretches. This separated form is known as the Valanis-Landel hypothesis [24, 36]. Using this form, the derivatives of Ψ with respect to the stretches are:

$$\frac{\partial \Psi}{\partial \lambda_i} = \frac{\partial \omega(\lambda_i)}{\partial \lambda_i} = \sum_{p=1}^{N} \mu_p \lambda_i^{\alpha_p - 1}, \tag{79}$$

$$\frac{\partial^2 \Psi}{\partial \lambda_i \partial \lambda_j} = \delta_i^j \frac{\partial^2 \omega(\lambda_i)}{\partial \lambda_i^2} = \delta_i^j \sum_{p=1}^{N} \mu_p \lambda_i^{\alpha_p - 2}(\alpha_p - 1). \tag{80}$$

From which again the stress and material tensors can be derived using Eqs. (70), (71) and (77).

4.3. Compressible Material Models

Similar to the compressible invariant-based formulation (Section 3.3), $\mathbf{S}$ and $\mathbb{C}$ for compressible material models will be derived for stretch-based material models. This means that the thickness-correction is applied iteratively. On the stretch-based terms of the stress and material tensors, that will be derived in this section, a transformation from the eigenvector space to the undeformed covariant tensor basis is required (Section 5.3) is applied to transform the material model to the curvilinear basis. Using the transformed stretch-based quantities, the same iterative procedure as in Section 3.3 can be used to converge towards the compressible stress and material tensors. Static condensation (Eq. (27)) is performed before transforming the material tensor.

For computation of the stress and material tensors, the relations in Eqs. (60) and (61) are used. As described in Section 3.3, the strain energy density function Ψ for compressible materials can be decomposed in an isochoric and volumetric part (see Eq. (48)) [30]. For stretch-based forms, this implies:

$$\Psi(\boldsymbol{\lambda}) = \Psi_{\text{iso}}(\dot{\boldsymbol{\lambda}}) + \Psi_{\text{vol}}(J). \tag{81}$$

The stretches $\dot{\lambda}_i$ are the modified principal stretches, defined as:

$$\dot{\lambda}_i := J^{-\frac{1}{3}} \lambda_i. \tag{82}$$

Using Eq. (82), any volumetric strain energy density function for incompressible materials can be transformed to its compressible material equivalent by substitution of Eq. (82) into Eq. (81) and by selecting an volumetric component Ψ_{vol}.

Example 4 (*Compressible Ogden Material Model*)**.** The compressible Ogden material model can be derived by substituting Eq. (82) into Eq. (78):

$$\Psi = \sum_{p=1}^{N} \frac{\mu_p}{\alpha_p} J^{-\frac{1}{3}} \left(\lambda_1^{\alpha_p} + \lambda_2^{\alpha_p} + \lambda_3^{\alpha_p} - 3 \right) + \Psi_{\text{vol}}. \tag{83}$$

In this equation, Ψ_{vol} can be chosen according to Eq. (52) but is not specified in the further

derivation. Using this form, the derivatives of Ψ with respect to the stretches are:

$$\frac{\partial \Psi}{\partial \lambda_i} = \sum_{p=1}^{N} \frac{\mu_p}{\alpha_p} \left[\frac{\partial \left(J^{-\frac{\alpha_p}{3}} \right)}{\partial \lambda_i} (\Lambda - 3) + J^{-\frac{\alpha_p}{3}} \alpha_p \lambda_i^{\alpha_p - 1} \right] + \frac{\partial \Psi_{\text{vol}}}{\partial \lambda_i} \tag{84}$$

$$= \sum_{p=1}^{N} \mu_p J^{-\frac{\alpha_p}{3}} \left[\lambda_i^{\alpha_p - 1} - \frac{1}{3\lambda_i} (\Lambda - 3) \right] + \frac{\partial \Psi_{\text{vol}}}{\partial \lambda_i}, \tag{85}$$

$$\frac{\partial^2 \Psi}{\partial \lambda_i \partial \lambda_j} = \sum_{p=1}^{N} \mu_p \left[\frac{\partial \left(J^{-\frac{\alpha_p}{3}} \right)}{\partial \lambda_i} (\Lambda - 3) + J^{-\frac{\alpha_p}{3}} \left(\delta_i^j \left((\alpha_p - 1) \lambda_i^{\alpha_p - 2} - \frac{1}{3} \lambda_i^{-2} (\Lambda - 3) \right) - \frac{1}{3\lambda_i} \alpha_p \lambda^{\alpha_p - 1} \right) \right]$$
$$+ \frac{\partial^2 \Psi_{\text{vol}}}{\partial \lambda_i \partial \lambda_j} \tag{86}$$

$$= \sum_{p=1}^{N} \mu_p J^{-\frac{\alpha_p}{3}} \left[\frac{\alpha_p}{3} \left(\frac{\Lambda}{3\lambda_i \lambda_j} - \frac{\lambda_a^{\alpha_p - 1}}{\lambda_b} - \frac{\lambda_b^{\alpha_p - 1}}{\lambda_a} \right) + \delta_i^j \left((\alpha_p - 1) \lambda_i^{\alpha_p - 1} + \frac{\Lambda}{3\lambda_i^2} \right) \right] + \frac{\partial^2 \Psi_{\text{vol}}}{\partial \lambda_i \partial \lambda_j}, \tag{87}$$

where $\Lambda = \lambda_1^{\alpha_p} + \lambda_2^{\alpha_p} + \lambda_3^{\alpha_p}$.

5. Implementation Aspects

In order to provide some implementation aspects for the presented formulations (Section 4), the assembly of the nonlinear system for isogeometric Kirchhoff-Love shells will be recalled (Section 5.1) as well as the computation of the eigenvalues and eigenvectors of the deformation tensor $\mathbf{C}$ (Section 5.2). Lastly, we will provide details about the transformation of the stress and material tensors $\mathbf{S}$ and $\mathbb{C}$ from spectral to curvilinear bases (Section 5.3).

5.1. System Assembly

For the implementation of Kirchhoff-Love shells recall that the vector of internal forces and the tangential stiffness matrix read [10, 12]:

$$F_r^{\text{int}} = \int_\Omega \left(\bar{\mathbf{n}}^\top \frac{\partial \bar{\varepsilon}}{\partial u_r} + \bar{\mathbf{m}}^\top \frac{\partial \bar{\kappa}}{\partial u_r} \right) \mathrm{d}\Omega \,, \tag{88}$$

$$K_{rs} = \int_\Omega \left(\left(\bar{\mathbf{D}}^0 \frac{\partial \bar{\varepsilon}}{\partial u_s} + \bar{\mathbf{D}}^1 \frac{\partial \bar{\kappa}}{\partial u_s} \right) \frac{\partial \bar{\varepsilon}}{\partial u_r} + \bar{\mathbf{n}}^\top \frac{\partial^2 \bar{\varepsilon}}{\partial u_r \partial u_s} + \left(\bar{\mathbf{D}}^1 \frac{\partial \bar{\varepsilon}}{\partial u_s} + \bar{\mathbf{D}}^2 \frac{\partial \bar{\kappa}}{\partial u_s} \right) \frac{\partial \bar{\varepsilon}}{\partial u_r} + \bar{\mathbf{m}}^\top \frac{\partial^2 \bar{\kappa}}{\partial u_r \partial u_s} \right) \mathrm{d}\Omega \,. \tag{89}$$

Here, we note that the matrices $\bar{\mathbf{D}}^k$, $k = 0, 1, 2$, are k^{th} thickness moments of the material tensor represented as a 3×3 matrix and $\bar{\mathbf{n}}$ and $\bar{\mathbf{m}}$ are the zero-th and first thickness moments of the stress tensor, see [12]. The thickness integrals are, in the present paper and in [12], computed using numerical through-thickness integration with four Gaussian points. As discussed before by [15], the matrices $\bar{\mathbf{D}}^1$ can differ in the variations of the normal force tensor $\bar{\mathbf{n}}$ and the moment tensor $\bar{\mathbf{m}}$ depending the analytic projected or directly decoupled alternatives for thickness integration.

5.2. Eigenvalue Computation

The eigenvalues a tensor quantity can be computed by solving Eq. (17) or, alternatively, by computing the eigenvalues of the matrix that results from symbolic computation of $\mathbf{C} = C_{ij}\mathring{\mathbf{g}}_i \otimes \mathring{\mathbf{g}}_j$. Since $\lambda_3^2 = \sqrt{C_{33}}$ is decoupled by construction, the other two eigenvalues λ_1^2 and λ_2^2 are to be computed. Here, an basic routine for the eigenvalues and eigenvectors for 3×3 matrices is employed on the matrix that follows from explicit computation of $\mathbf{C} = C_{\alpha\beta}\, \mathring{\mathbf{g}}_\alpha \otimes \mathring{\mathbf{g}}_\beta$.

5.3. Tensor Transformation

Since the stretch-based stress and material tensor are derived in spectral form (i.e. in the eigenvector space) a transformation towards the curvilinear basis needsis required in order to use these entities in further computations. Recall that the spectral forms of $\mathbf{S}$ and $\mathbb{C}$ are:

$$\mathbf{S} = S^i\, \mathbf{v}_i \otimes \mathbf{v}_i, \quad \mathbb{C} = \mathbb{C}^{ijkl}\, \mathbf{v}_i \otimes \mathbf{v}_j \otimes \mathbf{v}_k \otimes \mathbf{v}_l. \tag{90}$$

The the invariant-based stress and material tensors are defined in the curvilinear basis, as follows:

$$\mathbf{S} = S^{ij}\, \mathring{\mathbf{g}}_i \otimes \mathring{\mathbf{g}}_j \quad \mathbb{C} = \mathbb{C}^{ijkl}\, \mathring{\mathbf{g}}_i \otimes \mathring{\mathbf{g}}_j \otimes \mathring{\mathbf{g}}_k \otimes \mathring{\mathbf{g}}_l. \tag{91}$$

Since the strain tensors (c.f. Eq. (19)) are defined in the curvilinear basis, it is convenient to define the quantities in the variational form (c.f. Eq. (20)) defined in the curvilinear basis. Hence, the stretch-based stress and material tensors have to be transformed to the undeformed covariant curvilinear basis by:

$$\begin{aligned} \tilde{S}^{ij} &= S^{pq}(\mathbf{v}_p \cdot \mathring{\mathbf{g}}_i)(\mathbf{v}_q \cdot \mathring{\mathbf{g}}_j), \\ \tilde{\mathbb{C}}^{ijkl} &= \mathbb{C}^{pqrs}(\mathbf{v}_p \cdot \mathring{\mathbf{g}}_i)(\mathbf{v}_q \cdot \mathring{\mathbf{g}}_j)(\mathbf{v}_r \cdot \mathring{\mathbf{g}}_k)(\mathbf{v}_s \cdot \mathring{\mathbf{g}}_l), \end{aligned} \tag{92}$$

where $\tilde{S}^{ij}$ and $\tilde{\mathbb{C}}^{ijkl}$ are the coefficients of the stress and material tensors in the curvilinear basis.

Obviously, the tensor transformation only needs to be computed for non-zero components of $\mathbb{C}^{pqrs}$. For incompressible material models, static condensation is applied analytically, which implies that the transformations only need to be applied for indices ranging from $\alpha, \beta, \gamma, \delta = 1, 2$, thus the transformation consists of mapping $2^4 = 16$ entries. However, it is known that for hyperelastic materials the contravariant components of the material tensor, $\mathbb{C}^{ijkl}$, posses minor and major symmetry [24, 25], i.e.

$$\mathbb{C}^{abcd} = \mathbb{C}^{bacd} = \mathbb{C}^{abdc} \qquad \text{minor symmetry,} \tag{93}$$

$$= \mathbb{C}^{cdab} \qquad \text{major symmetry,} \tag{94}$$

So that only six unique components exists for the $2 \times 2 \times 2 \times 2$ tensor. Furthermore, Eq. (61) implies that the non-zero components of $\mathbb{C}^{ijkl}$ are of the form $\mathbb{C}^{iiii}$, $\mathbb{C}^{iijj}$, $\mathbb{C}^{ijij}$ and $\mathbb{C}^{ijji}$ of which the last two are equal by virtue of the minor symmetry property. This implies that the $2\times2\times2\times2$ tensor has only four uniquely defined components, namely $\mathbb{C}^{1111}$, $\mathbb{C}^{1122}$, $\mathbb{C}^{2222}$ and $\mathbb{C}^{1212}$.

For compressible material models, static condensation is applied in the spectral basis, i.e. on the tensor $\mathbb{C}$ before it is transformed to the covariant undeformed tensor basis. From Eq. (27) we see that the static condensation procedure requires the computation of $\mathbb{C}^{3333}$, $\mathbb{C}^{\alpha\beta33}$ and $\mathbb{C}^{33\alpha\beta}$, where the last two are equal by virtue of the major symmetry property. Using the minor and

major symmetries again, this implies computation of four extra (unique) components, namely $\mathbb{C}^{1133}$, $\mathbb{C}^{2233}$, $\mathbb{C}^{1233}$ and $\mathbb{C}^{3333}$.

Accordingly, it can be concluded that for incompressible materials four and for compressible materials eight unique components of the spectral material tensor need to be computed, when exploiting minor and major symmetry, as well as the nature of Eq. (61). Hence, the additional costs of the transformation are existent, but limited due to symmetries of the spectral form.

6. Numerical experiments

For benchmarking purposes, the results of five numerical experiments have been used for verification and validation of the presented formulations for incompressible and compressible material models. For the uniaxial tension and pressurized balloon benchmarks (Sections 6.1 and 6.3, respectively), analytical solutions are available, meaning the results will serve as verification of the stretch-based material model formulations. The restrained sheet elongation (Section 6.2) will serve as validation of the stretch-based material model formulations because of the involved numerical (IGA and FEM) and experimental data. The benchmark of the pinched cylinder (Section 6.4) provides additional comparison of selected material models with reference works. In order to verify the presented isogemetric Kirchhoff-Love formulation for a stretch-based Ogden material with its FEM couterpart, the conical shell collapse (Section 6.5) is incorporated. The described models have been implemented in the open-source library G+Smo (Geometry + Simulation Modules) [37].

In the numerical experiments, compressible and incompressible formulations of the Neo-Hookean (NH), Mooney-Rivlin (MR) and Ogden (OG) material models have been used. The Neo-Hookean models are given by:

$$\Psi(\mathbf{C}) = \frac{\mu}{2}\Big(J^{-\frac{2}{3}} I_1 - 3\Big) + \Psi_{\text{vol}}(J) \qquad \text{NH Compressible,} \tag{95}$$

$$\Psi(\mathbf{C}) = \frac{\mu}{2}(I_1 - 3) \qquad \text{NH Incompressible.} \tag{96}$$

For the MR and OG models, the established formulations (respectivelyEqs. (38) and (51) and Eqs. (78) and (83)) are used. For all models, the following volumetric part of the strain energy density function is adopted (see Eq. (52)):

$$\Psi_{\text{vol}} = K\mathcal{G}(J) = K\beta^{-2}\Big(\beta \log(J) + J^{-\beta} - 1\Big). \tag{97}$$

For the NR and MR models, the invariants can be replaced by Eqs. (14) to (16) to obtain stretch-based forms (see also Appendix B). Unless stated otherwise, for the compressible models $\beta = -2$, and for the Mooney-Rivlin model $c_1/c_2 = 7$ [29] is used. For the Ogden model the coefficients from [38] are re-scaled to the value of μ:

$$\begin{aligned} \mu_1 &= \frac{6.300}{\mu_0}\mu, \quad & \alpha_1 &= 1.3, \\ \mu_2 &= \frac{0.012}{\mu_0}\mu, \quad & \alpha_2 &= 5.0, \\ \mu_3 &= -\frac{0.100}{\mu_0}\mu, \quad & \alpha_3 &= -2.0, \end{aligned} \tag{98}$$

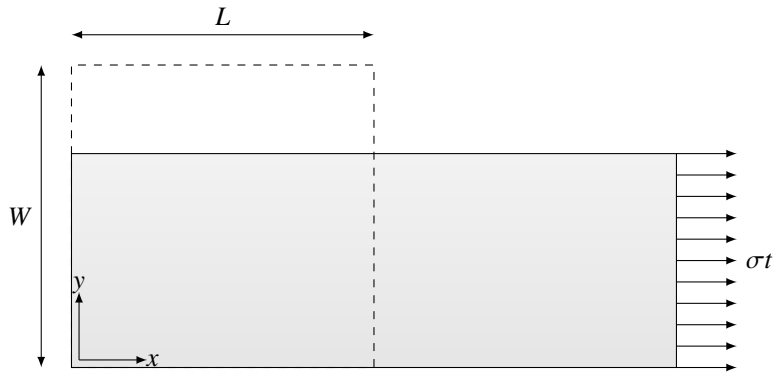

Figure 1: Geometry for the uniaxial tension case. The filled geometry represents the undeformed configuration and the dashed line indicates the undeformed geometry. The bottom side of the undeformed sheet is fixed in y-direction and the left side of the sheet is fixed in x-direction. The applied load is σt where σ is the actual Cauchy stress and t is the thickness of the sheet.

where $\mu_0 = 4.225$. Lastly, for obtaining the analytical solutions, we note that the principal Cauchy stresses are defined as :

$$\sigma_i = J^{-1}\lambda_i \frac{\partial \Psi}{\partial \lambda_i}. \tag{99}$$

6.1. Uniaxial Tension

The first benchmark case is uniaxial tension of a material block. In this case, a block with dimensions $L{\times}W{\times}t = 1{\times}1{\times}0.001[\mathrm{m}^2]$ is considered. The shear modulus is $\mu = E/(2(1+\nu))$ where E and ν are the Young's modulus and Poisson ratio, respectively, such that $\mu = 1.5 \cdot 10^6$ [N/m^2]. The block is modeled by shell elements, which means that the $L \times W$ plane is considered and all edges are restrained in vertical direction ($z = 0$). The left edge ($x = 0$) is restrained in x direction and on the right edge ($x = L$) a distributed load σt is applied. The bottom edge ($y = 0$) is restrained in y direction and the top edge ($y = B$) is free to move (see Fig. 1.

For incompressible materials, the analytical solution is obtained by the incompressibility constraint $J = \lambda_1\lambda_2\lambda_3 = 1$ and $\lambda_1 = \lambda$ as the stretch of the block. As a consequence, $\lambda_2 = \lambda_3 = 1/\sqrt{\lambda}$ are the changes in width and thickness of the block and the Cauchy-stresses are $\sigma_2 = \sigma_3 = 0$ and

$$\begin{aligned}
\text{Neo-Hookean:} \quad & \sigma_1 = \sigma = \mu\left(\lambda^2 - \lambda^{-1}\right), \\
\text{Mooney-Rivlin:} \quad & \sigma_1 = \sigma = c_1\left(\lambda^2 - \lambda^{-1}\right) + c_2\left(\lambda - \lambda^{-2}\right), \\
\text{Ogden:} \quad & \sigma_1 = \sigma = \sum_{p=1}^{N} \mu_p\left(\lambda^{\alpha_p} - \lambda^{\frac{\alpha_p}{2}}\right).
\end{aligned} \tag{100}$$

For compressible materials, the incompressibility constraint is not valid, hence $J = \lambda_1\lambda_2\lambda_3 \neq 1$, and $\lambda_1 = \lambda$ and $\lambda_2 = \lambda_3 = \sqrt{J/\lambda}$. The plane-stress condition $\sigma_3 = 0$ using Eq. (100) is adopted to obtain J for any value of λ. Using this result, the Cauchy-stress for any λ can then be obtained

Table 1: Residual norms per iteration for the 10^{th} load-step for uniaxial tension for all material models in compressible and incompressible forms. For the Neo-Hookean and Mooney-Rivlin models, the iteration residuals are provided for the stretch-based and invariant-based implementations. For the Ogden model, only the results for the stretch-based implementation are given, since no invariant-based formulation exists. For the Neo-Hookean and Mooney-Rivlin models, results are only observed in the last iteration, due to machine precision of the arithmetic.

	Iteration	Neo-Hookean		Mooney-Rivlin		Ogden
		Stretch	Invariant	Stretch	Invariant	Stretch
Incomp.	1	$1.8799 \cdot 10^{-4}$	$1.8799 \cdot 10^{-4}$	$3.9993 \cdot 10^{-3}$	$3.9993 \cdot 10^{-3}$	$1.6073 \cdot 10^{-3}$
	2	$1.0523 \cdot 10^{-6}$	$1.0523 \cdot 10^{-6}$	$2.2532 \cdot 10^{-5}$	$2.2532 \cdot 10^{-5}$	$2.0652 \cdot 10^{-7}$
	3	$3.3816 \cdot 10^{-11}$	$3.3816 \cdot 10^{-11}$	$7.2294 \cdot 10^{-10}$	$7.2294 \cdot 10^{-10}$	$8.2372 \cdot 10^{-13}$
	4	$2.6535 \cdot 10^{-16}$	$2.8834 \cdot 10^{-16}$	$2.3197 \cdot 10^{-15}$	$5.1781 \cdot 10^{-16}$	$2.3283 \cdot 10^{-15}$
Comp.	1	$1.6073 \cdot 10^{-03}$	$1.6073 \cdot 10^{-03}$	$2.0643 \cdot 10^{-03}$	$2.0643 \cdot 10^{-03}$	$1.60731 \cdot 10^{-3}$
	2	$2.0652 \cdot 10^{-7}$	$2.0652 \cdot 10^{-7}$	$2.7452 \cdot 10^{-6}$	$2.7452 \cdot 10^{-6}$	$2.0652 \cdot 10^{-7}$
	3	$8.2372 \cdot 10^{-13}$	$8.2254 \cdot 10^{-13}$	$1.2340 \cdot 10^{-11}$	$1.2340 \cdot 10^{-11}$	$8.2372 \cdot 10^{-13}$
	4	$2.3283 \cdot 10^{-15}$	$4.8586 \cdot 10^{-16}$	$2.1144 \cdot 10^{-15}$	$6.9650 \cdot 10^{-16}$	$2.32830 \cdot 10^{-15}$

using:

$$
\begin{aligned}
\text{Neo-Hookean:} \quad & \sigma_1 = \sigma = \frac{2}{3}\mu J^{\frac{2}{3}}\left(\lambda^2 J^{-1} - \lambda^{-1}\right) + \frac{K}{2}\left(J - J^{-1}\right), \\
\text{Mooney-Rivlin:} \quad & \sigma_1 = \sigma = \frac{2}{3}c_1 J^{\frac{2}{3}}\left(\lambda^2 J^{-1} - \lambda^{-1}\right) + \frac{4}{3}c_2 J^{\frac{1}{3}}\left(\lambda J^{-1} - \lambda^{-2}\right) + \frac{K}{2}\left(J - J^{-1}\right), \\
\text{Ogden:} \quad & \sigma_1 = \sigma = \sum_{p=1}^{N}\left[\frac{2}{3}\frac{\mu_p}{J}\left(\left(\lambda J^{-\frac{1}{3}}\right)^{\alpha_p} - \left(\lambda^{-1} J^{\frac{2}{3}}\right)^{\frac{\alpha_p}{2}}\right)\right] + \frac{K}{2}\left(J - J^{-1}\right).
\end{aligned}
\tag{101}
$$

In Fig. 2 the results for uniaxial tension are depicted. The numerical and analytical solutions for incompressible and compressible materials show a perfect match for all quantities studied (thickness decrease λ_3, axial Cauchy stress σ and Jacobian determinant J). Note that the Jacobian determinant for incompressible materials is equal to 1 and hence not shown. The residual norms of the non-linear iteration convergence for the invariant-based and stretch-based Neo-Hookean and Mooney-Rivlin models as well as the stretch-based Ogden model are equal in all iterationsTable 1, showing that the present formulation provides exactly the same rates of convergence as the invariant-based method. Last but not least, the iterations converge with the second order, as can be expected when using Newton iterations.

6.2. Restrained Sheet Elongation

Related to the first benchmark in the work of [15] and on the experiments of [39], a tensile load is applied on a strip of which the short edges are fixed and the long edges are free (see Fig. 3). Focus is on the non-domensional load versus end-point displacement in longitudinal (load and displacement) direction. For incompressible materials, comparison is made with the numerical results of [15] and for compressible materials, comparison is made with the experimental and numerical results of [39]. In both cases, the geometric parameters of the sheet are $L = 157.895$ [mm], $W = 78.947$ [mm] and $t = 0.15$ [mm] leading to $L/W = 2$ and $t/W = 1.90{\cdot}10^{-3}$ as in [39]. Furthermore, for comparison with [15] Young's modulus $E = 1$[Pa]], and a Poisson's ratio $\nu = 0.5$ (due to incompressibility) are used, which leads to $\mu = 1/3$[Pa]. For the Mooney-Rivlin model, $c_1/c_2 = 1/2$ such that $c_1 = 1/9$ and $c_2 = 2/9$. Scaling according to

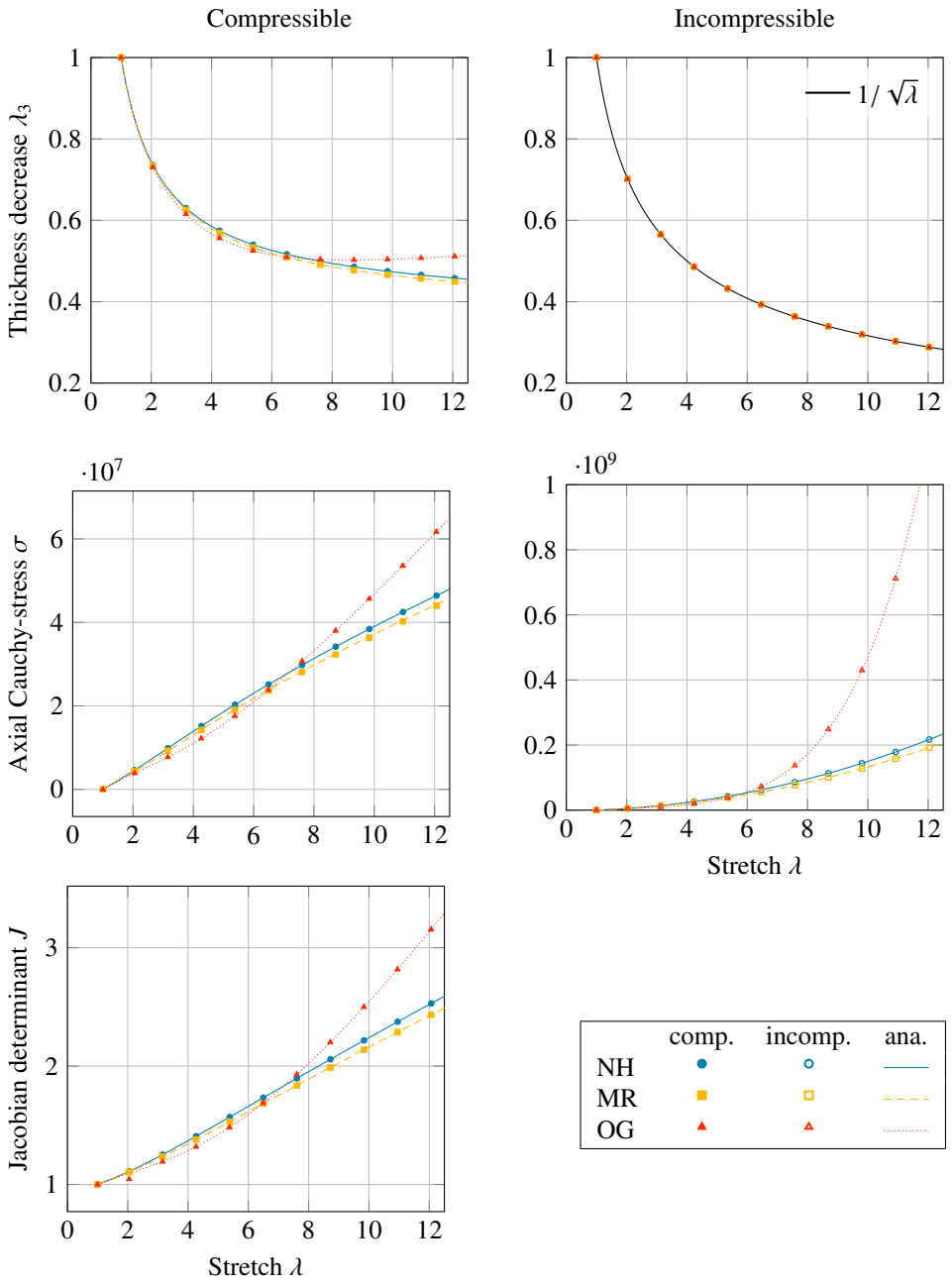

Figure 2: Results for uniaxial tension for compressible (left column) and incompressible materials (right column); where the first row presents the thickness decrease λ_3, the second row the axial Cauchy stress or true axial stress σ and the last row the Jacobian determinant J for compressible materials; all against the stretch λ. The material models that are used are the Neo-Hookean (NH) the Mooney-Rivlin (MR) and the Ogden (OG) material models

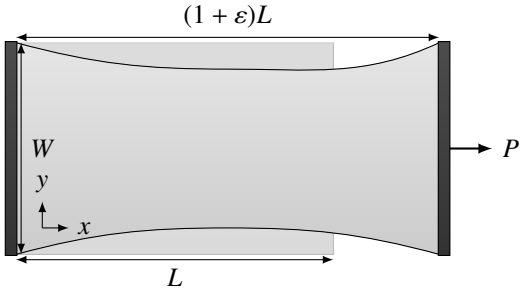

Figure 3: Modeling geometry for the uniaxially loaded restrained sheet.

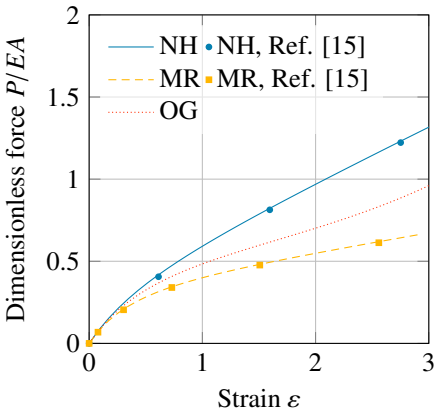

Figure 4: Uniaxial tension of a restrained sheet using incompressible material models. The reference results are obtained from the work of [15], specifically for their directly decoupled method. The dimensionless force is obtained by normalization of the applied force P by the Young's modulus E and the cross sectional area A.

Eq. (98) is applied for the Ogden material model. For the sake of comparison with [39], a Neo-Hookean material model with Young's modulus 1 [Pa] and Poisson ratio $\nu = 0.45$ is adopted. In the comparison with the data from [15] 16×8 quadratic B-spline elements are used and for comparison with [39] 32×16 cubic elements are used.

A good match with the results of [15] for the incompressible Neo-Hookean and Mooney-Rivlin models can be seen in Fig. 4. Note that the forces in the reference paper are normalized by $E = 3c_1$ for both the Neo-Hookean and Mooney-Rivlin models, whereas in the present simulations, the are normalized by $E = 3\mu$ (since $\nu = 0.5$ in the comparison with [15]). Furthermore, the deflection contour at the sheet sides (Fig. 5) shows a good agreement with the numerical/experimental results of [39] as well. The curves are presented for different strains which shows that dispite strain-normalization on the vertical axis strain dependence is still visible, meaning that there is non-linear dependence of the strains in the scaling laws.

6.3. Pressurized Balloon

The response affected pressure of a spherical balloon is used for benchmarking purposes as well. The analytical pressure formulation denotes [24]:

$$p = 2\frac{t}{R}\sigma, \tag{102}$$

where h and r are the undeformed thickness and radius of the balloon, respectively, $\sigma_1 = \sigma_2 = \sigma$ since $\lambda_1 = \lambda_2 = \lambda$ and $\lambda_3 = 1/\lambda$ by the incompressibility condition. Substituting in Eq. (99) yields σ, which can be substituted in Eq. (102) to obtain the internal pressure. For the Ogden

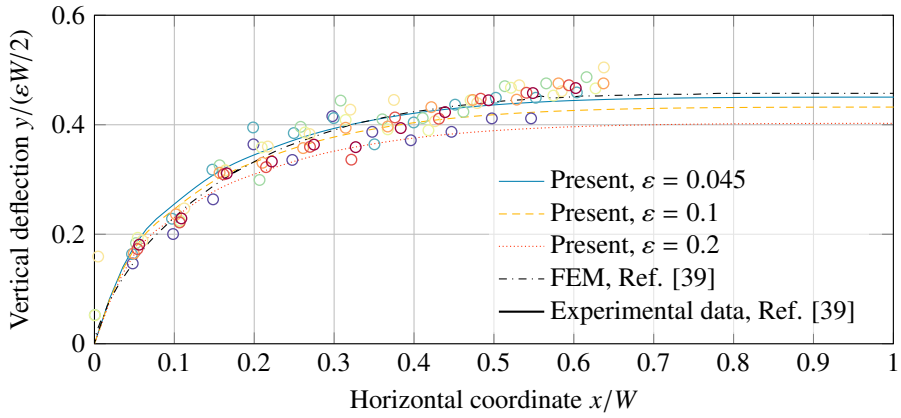

Figure 5: Poisson-effect of a stretched restrained sheet under uniaxial tension with $L/W = 2$, $T/W = 1.9 \cdot 10^{-3}$, $t = 0.15$ [mm], using the compressible Neo-Hookean model. The horizontal axis denotes the non-dimensional location on the length of the sheet and the vertical axis denotes the contraction over the width-axis, made nondimensional using the applied strain ε and the width of the sheet. The markers denote the experimental data from Ref. [39] and the markers are grouped on strain level ($\varepsilon \sim 0.09 - 0.30$) and colored using the same colors as in their work. The black dashed line denotes the result of the FEM model used by [39]. The other lines represent present results for different meshes on $\varepsilon \sim 0.1$.

material model, this yields:

$$\begin{aligned} \text{Neo-Hookean:} \quad & p = 2\frac{t}{R}\frac{\mu}{\lambda}\left(1-\lambda^{-6}\right), \\ \text{Mooney-Rivlin:} \quad & p = 2\frac{t}{R}\left(\frac{c_1}{\lambda}\left(1-\lambda^{-6}\right)\right) + \frac{c_2}{\lambda}\left(\lambda^{-6}-\lambda\right), \\ \text{Ogden:} \quad & p = 2\frac{t}{R}\sum_{p=1}^{N}\mu_p\left(\lambda^{\alpha_p-3}-\lambda^{-2\alpha_p-3}\right). \end{aligned} \tag{103}$$

The numerical model results are based on follower pressures, i.e. $\mathbf{f} = p\mathbf{n}$ where $\mathbf{n}$ is the unit normal in the current configuration. The balloon is modeled as a quarter sphere, of which the bottom point is fixed in all directions, and on the sides a symmetry condition is applied by clamping the sides in normal direction and restriction deflections orthogonal to the symmetry boundary (see Fig. 6). The geometry is modelled by 4 elements over the height and 2 element over the quarter-circumference, both of quadratic order.

For $R = 10$ [m], $t = 0.1$ [m] and $\mu = 4.2255 \cdot 10^5$ [N/m^2], a perfect agreement is obtained for all presented material models in comparison to the analytical solutions Fig. 7.

6.4. Pinched Cylinder

The response of a pinched cylinder (Fig. 8) [12, 40–42] is also benchmarked. Although the response is bending dominated - meaning the influence of Ogden materials is expected to be minimal - the present model is benchmarked for a variety of material models for the sake of completeness. The geometry of the problem is depicted in Fig. 8. The dimensions include

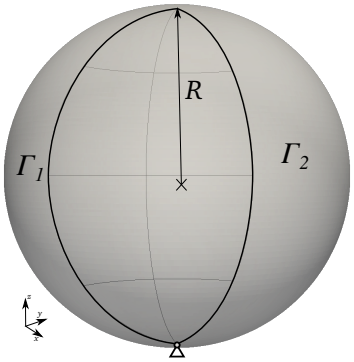

Figure 6: Geometry of the inflated balloon with 4 quadratic elements over the height. Symmetry conditions are applied on the boundaries Γ_1 and Γ_2.

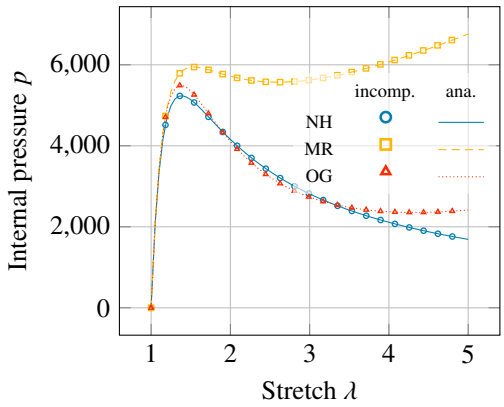

Figure 7: Inflation of a balloon. The vertical axis depicts the internally applied pressure and the horizontal axis depicts the stretch $\lambda_1 = \lambda_2 = \lambda$. The different lines and markers represent different material models, including Neo-Hookean (NH), Mooney-Rivlin (MR) and Ogden (OG). The radius of the sphere is $R = 10$ [m] and the thickness of the sphere $t = 0.1$ [m].

$L = 0.30$ [m], $R = 0.09$ [m] and $t = 2$ [mm]. Only a quarter of the geometry is modelled, by applying symmetry boundary conditions on the top and bottom edges Γ_1 and Γ_3 (y-displacements restrained and clamped edges) and on the mid-plane Γ_4 (x-displacement restrained and clamped edge). The bottom edge Γ_3 is restrained in the x and z directions as well. The geometry is meshed using 8×16 quartic shell elements. Furthermore, the material is represented by a compressible Neo-Hookean model

$$\Psi = \frac{\mu}{2}(I_1 - 3) - \mu \log(J) + \frac{\lambda}{4}\Big(J^2 - 1 - 2\log(J)\Big). \tag{104}$$

Here, $\mu = 60$[GPa] and $\lambda = 60$[GPa] represent the Lamé parameters and are equivalent to choosing $E = 168$ [GPa] and $\nu = 0.4$. It can be observed that this model is not based on the modified deformation tensor as in Eq. (44). In this paper, we furthermore model the benchmark with the compressible Neo-Hookean, Mooney-Rivlin and Ogden models from Eqs. (51), (83) and (B.4) to enrich the reference data for future benchmarking.

Fig. 10 presents the results of the pinched cylinder, with the vertical displacement of the endpoint A on the horizontal axis and the total applied load F on the cylinder (which is obtained by integrating f over Γ_1) on the vertical axis. The reference results are plotted for a vertical displacement of 0.16 [m]. We conclude that the results for the Neo-Hookean model of Eq. (104) correspond to the bounds of the reference results. Furthermore, the results with the models from Eqs. (51), (83) and (B.4) show marginal differences with the references and the influence of higher-order nonlinear material models (MR and OG) show minor differences as well; this is expected behaviour due to the bending dominated response. The minor difference with the isogeometric Kirchhoff-Love shell model of [12] is explained by the fact that the mesh size of the present study is slightly finer (16 vs. 12 elements over the half-circumference).

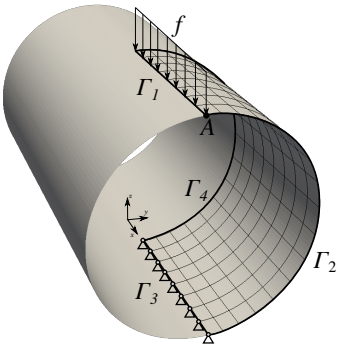

Figure 8: Geometry of the pinched cylinder with 8×16 quartic elements.

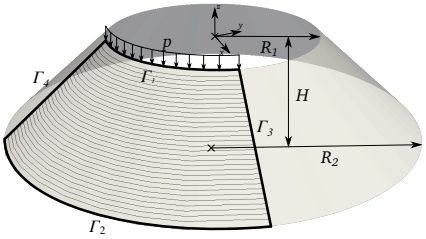

Figure 9: Geometry of the collapsing conical shell with 32 quadratic elements over the height.

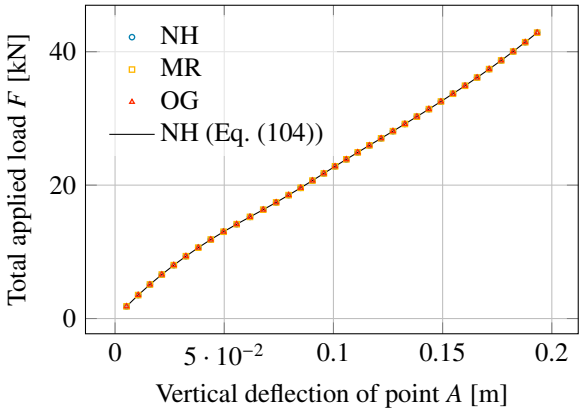

Model	F [kN]
Ref. [42]$_a$	34.59
Ref. [42]$_b$	34.66
Ref. [40]	34.71
Ref. [12]	34.86
Ref. [41]$_b$	35.12
Ref. [41]$_a$	35.47
Present (NH)	34.844
Present (MR)	34.840
Present (OG)	34.838
Present (NH, Eq. (104))	34.842

Figure 10: Results for the pinched cylinder with the vertical deflection on the horizontal axis and the total applied load on the vertical axis. The table on the right presents the relation of the present results with respect to reference results, where the present results are obtained with a 8×16 quartic isogeometric Kirchhoff-Love shell element on a quarter of the shell domain. All reference results employ the material model from Eq. (104). Ref [12] uses 16×12 quartic isogeometric Kirchhoff-Love shell elements and models half of the cylinder. Ref [41] uses (a) a 7-parameter model with exact strains; and (b) 6-parameter model with exact strains and an multiplicative strain-decomposition used in the incompatible mode method. Ref [42] employ solid-shell finite elements with (a) 1 element over the tickness; and with (b) 2 elements over the thickness. Ref [40] represents solutions obtained using finite elements with quadratic strains and a 7-parameter theory with condensation.

6.5. Conical Shell Collapse

A collapsing conical shell (or *frustrum*) is presented as a benchmark for modelling of strong non-linearities [8]. A conical shell with height $H = 1$ [m], top radius $r = 1$ [m], bottom radius $R = 2$ [m] and thickness $t = 0.1$ [m] as depicted in Fig. 9 is considered. The geometry is modelled with 32 quadratic elements over the height and one quadratic element over the circumference to represent axial symmetry. The corresponding material model is of the Ogden type and has the following parameters:

$$\begin{aligned} \mu_1 &= 6.300\ [\mathrm{N/m^2}], & \alpha_1 &= 1.3, \\ \mu_2 &= 0.012\ [\mathrm{N/m^2}], & \alpha_2 &= 5.0, \\ \mu_3 &= -0.100\ [\mathrm{N/m^2}], & \alpha_3 &= -2.0, \end{aligned}$$

implying that $\mu = 4.225\ [\mathrm{N/m^2}]$. Two sets of boundary conditions are considered for this geometry. In both sets the bottom of the shell (Γ_2) is hinged, hence the displacements are restricted in all directions. The top shell edge (Γ_1) is either kept rigid (no x and y displacements) or free, referred to as *constant* or *variable* radius, respectively [8]. On the top edge, a uniform load p is applied, providing a uniform displacement Δ. Due to symmetry, only one quarter of the geometry is modelled, which means that symmetry boundary conditions are applied on the $x = 0$ and $y = 0$ planes (Γ_3, Γ_4, see Fig. 9). The quarter-conical shell is modelled with 32 quartic shell elements over the width.

Loads are applied using displacement-control (DC) or arc-length control. In the former case, displacements are applied on the top-side of the cone and the deformation of the cone as well as the corresponding load on the top-boundary are computed. In the latter case, Crisfield's spherical arc-length procedure is used with extensions for resolving complex roots. If this method does not converge to an equilibrium point, the step size is bisected until a converged step is found. After this step, the step size is reset to its original value [43].

Figs. 11 and 12 present the result of the collapsing conical shell (constant and variable radius, respectively) of the present study and the reference results from [8]. The results for the displacement-controlled (DC) solution procedure shows that the different between the used material models are negligible, since the actual strains are relatively small. The results also agree with the displacement-controlled reference results of [8], and minor differences between the results might be a result of FE shear locking as involved for the reference results. Since more steps have been used for the displacement-controlled calculations, sharp corners in the curve can be observed for $\Delta \sim 1.9$ for constant radius and $\Delta \sim 1.8$ for variable radius.

An arc-length based calculation was used as well. From the results, one can observe revelation of the collapsing mechanism of the conical shell. For both cases (constant and variable radius) an almost anti-symmetric pattern in the load-deflection space can be observed, which initates and finishes at the kinks in the curve that was found with the displacement-control procedure. For the constant-radius shell, Fig. 11a shows two loops of large magnitude. In Figs. 11b and 12b it can be seen that collapsing behavior of the conical shell consists of states in which multiple *waves* in radial direction occur. For both cases, it can be seen that after the loops with the highest force-amplitude, the shell and its collapse-path invert and continue on the path that can be obtained with displacement-control.

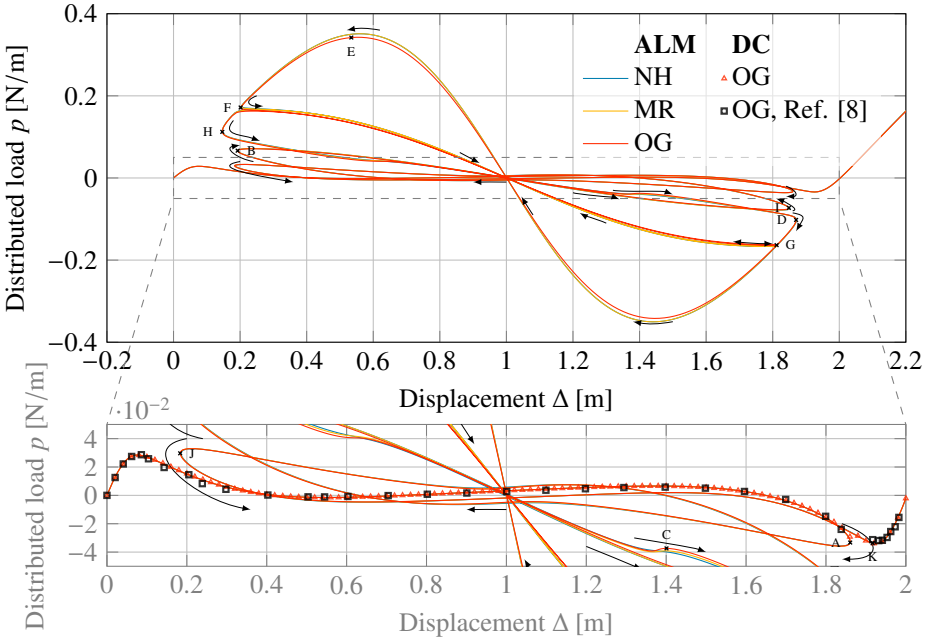

(a) Load-displacement diagram.

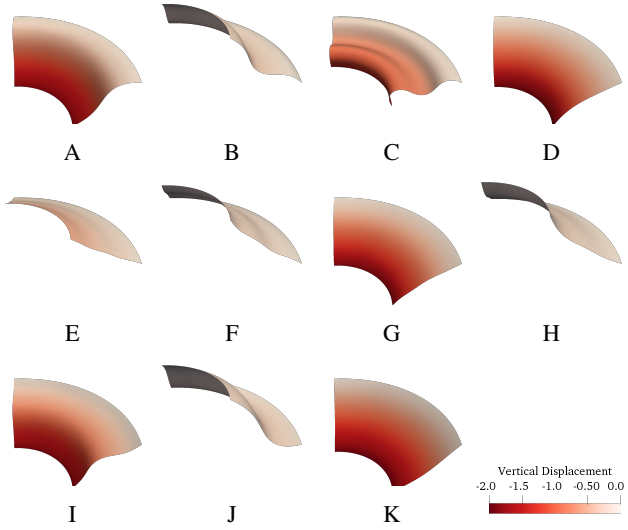

(b) Intermediate states of the frustrum

Figure 11: Result of the collapsing conical shell with *constant* radius;(a) load-displacement diagram,(b) undeformed geometries matching with the points indicated with capital letters in the diagram. The lines represent solutions obtained using the Arc-Length Method (ALM) and the markers represent solutions obtained by Displacement Control (DC). Note that the solution for the NH and MR models are overlapping on most parts of the path. The material models are Neo-Hookean (NH), Mooney-Rivlin (MR) and Ogden (OG). Since variation between the material models is rather small for the DC solutions, only the results for the OG material model are given. The reference results are obtained from [8]. A movie of the collapse is available as supplementary material to this paper (video 1).

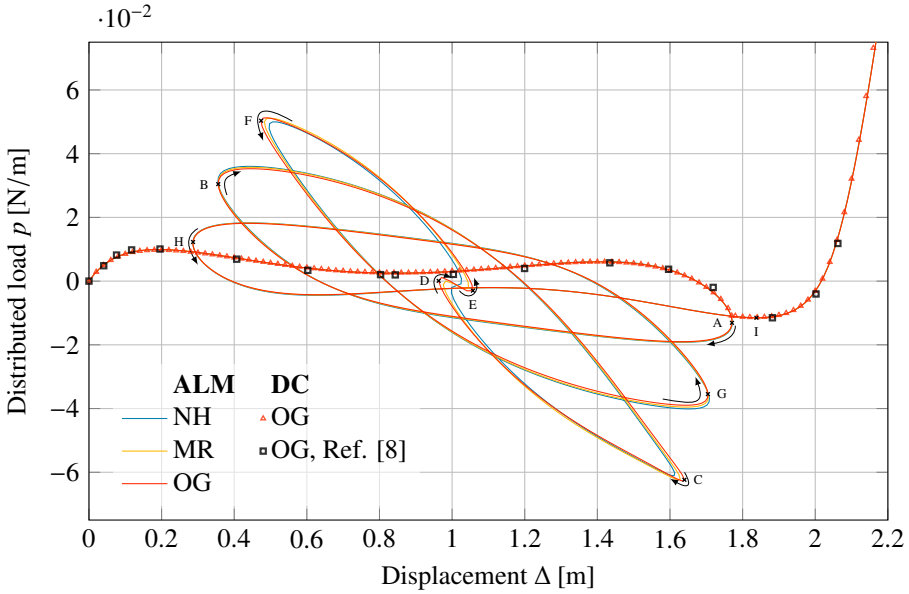

(a) Load-displacement diagram

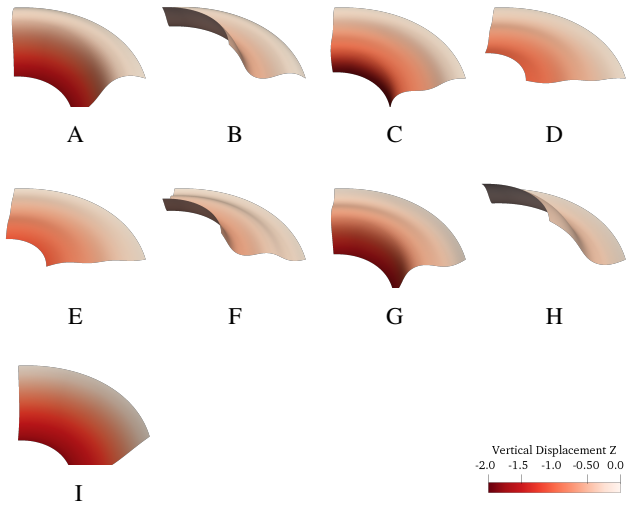

(b) Intermediate states of the frustrum

Figure 12: Result of the collapsing conical shell with *variable* radius; (a) load-displacement diagram, (b) undeformed geometries matching with the points indicated with capital letters in the diagram. The lines represent solutions obtained using the Arc-Length Method (ALM) and the markers represent solutions obtained by Displacement Control (DC). The material models are Neo-Hookean (NH), Mooney-Rivlin (MR) and Ogden (OG). Since variation between the material models is rather small for the DC solutions, only the results for the OG material model are given. The reference results are obtained from [8]. A movie of the collapse is available as supplementary material to this paper (video 2).

To the best of the author's knowledge, the collapsing of a collapsing conical shell was not investigated before. Complex load-displacement paths from Figs. 11a and 12a show that displacement-controlled simulations in this case ignore the collapsing behaviour of the shell with multiple limit points. The authors highly encourage further investigations on this benchmark for verification and validation.

7. Conclusions and recommendations

A stretch-based hyperelastic material formulation for isogeometric Kirchhoff-Love shells is presented, particularly useful when experimental material data fitting is involved to capture the model parameters. Complementing the existing invariant-based formulation [12], the implementation is based on a spectral decomposition of the stress and material tensors, which are transformed to the covariant curvilinear basis for consistency in the variational formulation. The eigenvalue computation and the transformation of the spectral entities imply additional computational costs, although limited due spectral material tensor symmetries. At the same time, the possibility to translate the stretch-based formulations into invariant-based ones is considered to be an advantage since it is not possible the other way around. There is still room for optimization of the eigenvalue computation, for instance by only evaluating the eigenvalues at the mid-plane of the shell.

For benchmarking purposes, incompressible and compressible Neo-Hookean, MOney-Rivlin and Ogden models have been considered; the latter being only defined in terms of stretches. Identical iteration residuals and correct convergence rates have been obtained. The analytical benchmarks (Sections 6.1 and 6.3) have shown a perfect agreement for the Ogden material model using the stretch-based formulation. Very good agreement was obtained for the numerical benchmarks. Benchmarking the response of a collapsing cylindrical shell, the displacement-controlled results are in good agreement. At the same time, a complex collapsing mechanism - not observed in literature before - was revealed when using the arc-length method.

Inspired by the results of the uniaxially stretched restrained sheet, we aim to further apply the present model on the modeling of wrinkling in our future work. The presented stretch-based formulation performance could be improved applying an analytical projection and direct decoupling [15] of the constitutive equations in order to prevent for numerical through-thickness integration (i.e. eigenvalue computations for all through-thickness Gaussian points).

Acknowledgments

The authors are grateful to Delft University of Technology for their support on this project. Also, HMV is grateful to the AROMATH department of Inria Sophia Antipolis - Méditerranée for hosting a two-month visit. Last but not least, the work of the developers on the Geometry + Simulation Modules (G+Smo) is greatly appreciated and this project could not have been executed without this.

Appendix A. Some useful derivatives

In this appendix, we provide the derivatives of the Jacobian determinant J, the invariants of the deformation tensor $\mathbf{C}$ and the inverse of the deformation tensor with respect to the components of $\mathbf{C}$, i.e. C_{ij}, as well as the stretches λ_i.

Appendix A.1. Derivatives with respect to the components of $\mathbf{C}$

Firstly, the derivatives of J are derived based on the derivative of J^2 [24], that is:

$$\frac{\partial J^2}{\partial C_{ij}} = \frac{\partial \det\{\mathbf{C}\}}{\partial C_{ij}} = \det\{\mathbf{C}\}\bar{C}^{ij} = J^2\bar{C}^{ij}, \tag{A.1}$$

which implies the derivative of J is:

$$\frac{\partial J}{\partial C_{ij}} = \frac{\partial J}{\partial J^2}\frac{\partial J}{\partial C_{ij}} = \frac{1}{2J}J^2\bar{C}^{ij} = \frac{1}{2}J\bar{C}^{ij}, \tag{A.2}$$

and the derivative of an arbitrary power $k \in \mathbb{R}$ of J is found by the chain rule:

$$\frac{\partial\left(J^k\right)}{\partial C_{ij}} = \frac{\partial\left(J^k\right)}{\partial J}\frac{\partial J}{\partial C_{ij}} = kJ^{k-1}\frac{1}{2}J\bar{C}^{ij} = \frac{k}{2}J^k\bar{C}^{ij}. \tag{A.3}$$

The second derivative of J is simply evaluated by taking the second derivative of Eq. (A.2). This gives:

$$\frac{\partial^2 J}{\partial C_{ij}\partial C_{kl}} = \frac{1}{4}J^2\bar{C}^{ij}\bar{C}^{kl} + \frac{1}{2}J\frac{\partial\bar{C}^{ij}}{\partial C_{kl}} = \frac{1}{4}\Big(J^2\bar{C}^{ij}\bar{C}^{kl} + J\Big(\bar{C}^{ik}\bar{C}^{jl} + \bar{C}^{il}\bar{C}^{jk}\Big)\Big), \tag{A.4}$$

where we used the derivative of an inverse of a tensor, from Eq. (2). From the definitions of the invariants in Eqs. (14) to (16) together with basic tensor identities from Eq. (2), we can evaluate

the derivatives of the invariants with respect to the components of $\mathbf{C}$:

$$\frac{\partial I_1}{\partial C_{\alpha\beta}} = \mathring{g}^{\alpha\beta}, \qquad \frac{\partial I_1}{\partial C_{33}} = 1, \tag{A.5}$$

$$\frac{\partial^2 I_1}{\partial C_{ij}\partial C_{kl}} = 0, \tag{A.6}$$

$$\frac{\partial I_2}{\partial C_{\alpha\beta}} = C_{33}\mathring{g}^{\alpha\beta} + J_0^2\bar{C}^{ij}, \frac{\partial I_2}{\partial C_{33}} = g_{\alpha\beta}\mathring{g}^{\alpha\beta}, \tag{A.7}$$

$$\begin{aligned}\frac{\partial^2 I_2}{\partial C_{\alpha\beta}\partial C_{\gamma\delta}} &= J_0^2\left(\bar{C}^{ij}\bar{C}^{kl} + \frac{\partial \bar{C}^{ij}}{\partial C_{kl}}\right)\\ &= J_0^2\left(\bar{C}^{ij}\bar{C}^{kl} - \frac{1}{2}\left(\bar{C}^{ik}\bar{C}^{jl} + \bar{C}^{il}\bar{C}^{jk}\right)\right),\end{aligned} \tag{A.8}$$

$$\frac{\partial^2 I_2}{\partial C_{\alpha\beta}\partial C_{33}} = \frac{\partial^2 I_2}{\partial C_{33}\partial C_{\alpha\beta}} = \mathring{g}^{\alpha\beta}, \qquad \frac{\partial^2 I_2}{\partial C_{33}^2} = 1, \tag{A.9}$$

$$\frac{\partial I_3}{\partial C_{\alpha\beta}} = \bar{C}^{\alpha\beta}, \qquad \frac{\partial I_3}{\partial C_{33}} = 1, \tag{A.10}$$

$$\frac{\partial^2 I_3}{\partial C_{\alpha\beta}\partial C_{\gamma\delta}} = -\frac{1}{2}\left(\bar{C}^{ik}\bar{C}^{jl} + \bar{C}^{il}\bar{C}^{jk}\right), \tag{A.11}$$

$$\frac{\partial^2 I_3}{\partial C_{33}^2} = \frac{\partial^2 I_3}{\partial C_{\alpha\beta}\partial C_{33}} = \frac{\partial^2 I_3}{\partial C_{33}\partial C_{\alpha\beta}} = 0. \tag{A.12}$$

Appendix A.2. Derivatives with respect to the stretches

We start by defining the derivatives of the Jacobian determinant. By definition, $J = \lambda_1\lambda_2\lambda_3$ and thus, the following holds for the derivative with respect to λ_i:

$$\frac{\partial J}{\partial \lambda_i} = \frac{J}{\lambda_i}. \tag{A.13}$$

The derivative of an arbitrary power k of J is:

$$\frac{\partial\left(J^k\right)}{\partial \lambda_i} = \frac{\partial\left(J^k\right)}{\partial J}\frac{\partial J}{\partial \lambda_i} = \frac{kJ^k}{\lambda_i},\ k \in \mathbb{R}, \tag{A.14}$$

and the second derivative of J is:

$$\frac{\partial^2 J}{\partial \lambda_i \partial \lambda_j} = \frac{J}{\lambda_i\lambda_j}. \tag{A.15}$$

Furthermore, from the definitions of the invariants in terms of stretches in Eqs. (14) to (16),

$$I_1 = \lambda_1^2 + \lambda_2^2 + \lambda_3^2, \tag{A.16}$$

$$I_2 = \lambda_1^2\lambda_2^2 + \lambda_2^2\lambda_3^2 + \lambda_1^2\lambda_3^2, \tag{A.17}$$

$$I_3 = \lambda_1^2\lambda_2^2\lambda_3^2, \tag{A.18}$$

we can easily evaluate their derivatives:

$$\frac{\partial I_1}{\partial \lambda_i} = 2\lambda_i, \tag{A.19}$$

$$\frac{\partial^2 I_1}{\partial \lambda_i \partial \lambda_j} = 2\delta_i^j, \tag{A.20}$$

$$\frac{\partial I_2}{\partial \lambda_i} = 2\lambda_i\Big(I_1 - \lambda_i^2\Big), \tag{A.21}$$

$$\frac{\partial^2 I_2}{\partial \lambda_i \partial \lambda_j} = 2\delta_i^j\Big(I_1 - \lambda_i^2\Big) + 4\Big(1 - \delta_i^j\Big)\lambda_i\lambda_j, \tag{A.22}$$

$$\frac{\partial I_3}{\partial \lambda_i} = 2\frac{I_3}{\lambda_i}, \tag{A.23}$$

$$\frac{\partial^2 I_3}{\partial \lambda_i \partial \lambda_j} = 2I_3\left(\frac{2}{\lambda_i\lambda_j} - \frac{\delta_i^j}{\lambda_i^2}\right). \tag{A.24}$$

Appendix B. Stretch-based material implementations

In this appendix, we briefly provide the derivatives of the strain energy density functions Ψ for the Neo-Hookean and Mooney-Rivlin models in the stretch-based context. In this way, they can be used for verification purpose of the stretch-based implementations.

Appendix B.1. Neo-Hookean Model

The strain energy density function for an incompressible Neo-Hookean material model is:

$$\Psi(\lambda_1, \lambda_2, \lambda_3) = \frac{\mu}{2}(I_1 - 3) = \frac{\mu}{2}\Big(\lambda_1^2 + \lambda_2^2 + \lambda_3^2 - 3\Big). \tag{B.1}$$

Using Eqs. (A.19) and (A.24) this gives:

$$\frac{\partial \Psi}{\partial \lambda_i} = \frac{\mu}{2}\frac{\partial I_1}{\partial \lambda_i} = \mu\lambda_i, \tag{B.2}$$

$$\frac{\partial^2 \Psi}{\partial \lambda_i \partial \lambda_j} = \frac{\mu}{2}\frac{\partial^2 I_1}{\partial \lambda_i \partial \lambda_j} = \mu\delta_i^j. \tag{B.3}$$

The strain energy density function for the compressible Neo-Hookean model is:

$$\Psi(\lambda_1, \lambda_2, \lambda_3) = \frac{\mu}{2}\Big(J^{-\frac{2}{3}} I_1 - 3\Big) = \frac{\mu}{2}\Big[J^{-\frac{2}{3}}\Big(\lambda_1^2 + \lambda_2^2 + \lambda_3^2\Big) - 3\Big] + K\beta^{-2}\Big(\beta\log(J) + J^{-\beta} - 1\Big). \tag{B.4}$$

using Eqs. (A.14), (A.19) and (A.24) this gives:

$$\frac{\partial \Psi}{\partial \lambda_i} = \mu J^{-\frac{2}{3}}\left(\lambda_i - \frac{1}{3}\frac{I_1}{\lambda_i}\right) + \frac{K}{\lambda_i\beta}\Big(1 - J^{-\beta}\Big), \tag{B.5}$$

$$\begin{aligned}\frac{\partial^2 \Psi}{\partial \lambda_i \partial \lambda_j} = {} & \mu J^{-\frac{2}{3}}\left(\frac{4}{9}\frac{I_1}{\lambda_i\lambda_j} - \frac{2}{3}\left(\frac{\lambda_j}{\lambda_i} + \frac{\lambda_i}{\lambda_j}\right) + \delta_i^j\left(2 + \frac{2}{3}\frac{I_1}{\lambda_a^2}\right)\right) \\ & + \frac{K}{\lambda_i\lambda_j\beta}\Big(\beta J^{-\beta} + \delta_i^j\Big(J^{-\beta} - 1\Big)\Big).\end{aligned} \tag{B.6}$$

Here, we used the volumetric strain energy density function Ψ_{vol} from Eq. (52).

Appendix B.2. Mooney-Rivlin Model

The strain energy density function for an incompressible Mooney-Rivlin material model is:

$$\Psi(\lambda_1,\lambda_2,\lambda_3) = \frac{c_1}{2}(I_1-3) + \frac{c_2}{2}(I_2-3) = \frac{c_1}{2}\Big(\lambda_1^2+\lambda_2^2+\lambda_3^2-3\Big) + \frac{c_2}{2}\Big(\lambda_1^2\lambda_2^2+\lambda_2^2\lambda_3^2+\lambda_1^2\lambda_3^2-3\Big). \tag{B.7}$$

Using Eqs. (A.19) and (A.24), the derivatives of this function with respect to the stretches can be written as:

$$\frac{\partial\Psi}{\partial\lambda_i} = \frac{c_1}{2}\frac{\partial I_1}{\partial\lambda_i} + \frac{c_2}{2}\frac{I_2}{\lambda_i} = c_1\lambda_i + c_2\lambda_i(I_1-\lambda_i^2), \tag{B.8}$$

$$\frac{\partial^2\Psi}{\partial\lambda_i\partial\lambda_j} = \frac{c_1}{2}\frac{\partial^2 I_1}{\partial\lambda_i\partial\lambda_j} + \frac{c_2}{2}\frac{I_2}{\lambda_i}\lambda_j = c_1\delta_i^j + c_2(I_1-\lambda_i^2)\delta_i^j + 2c_2\lambda_i\lambda_j(1-\delta_i^j). \tag{B.9}$$

The strain energy density function for the compressible Mooney-Rivlin model is:

$$\Psi(\lambda_1,\lambda_2,\lambda_3) = \frac{c_1}{2}\Big(J^{-\frac{2}{3}}I_1-3\Big) + \frac{c_2}{2}\Big(J^{-\frac{4}{3}}I_2-3\Big) \tag{B.10}$$

$$= \frac{c_1}{2}\Big[J^{-\frac{2}{3}}\Big(\lambda_1^2+\lambda_2^2+\lambda_3^2\Big)-3\Big] + \frac{c_1}{2}\Big[J^{-\frac{4}{3}}\Big(\lambda_1^2+\lambda_2^2+\lambda_3^2\Big)-3\Big] + K\beta^{-2}\Big(\beta\log(J)+J^{-\beta}-1\Big). \tag{B.11}$$

Using Eqs. (A.14), (A.19) and (A.24) this gives:

$$\frac{\partial\Psi}{\partial\lambda_i} = c_1J^{-\frac{2}{3}}\left(\lambda_i-\frac{1}{3}\frac{I_1}{\lambda_i}\right) + c_2J^{-\frac{4}{3}}\left(\Big(I_1-\lambda_i^2\Big)\lambda_i-\frac{2}{3}\frac{I_2}{\lambda_i}\right) + \frac{K}{\lambda_i\beta}\Big(1-J^{-\beta}\Big), \tag{B.12}$$

$$\begin{aligned}\frac{\partial^2\Psi}{\partial\lambda_i\partial\lambda_j} = {} & c_1J^{-\frac{2}{3}}\left(\frac{4}{9}\frac{I_1}{\lambda_i\lambda_j} - \frac{2}{3}\left(\frac{\lambda_j}{\lambda_i}+\frac{\lambda_i}{\lambda_j}\right) + \delta_i^j\left(2+\frac{2}{3}\frac{I_1}{\lambda_a^2}\right)\right)\\ & + c_2J^{-\frac{4}{3}}\left(\frac{16}{9}\frac{I_2}{\lambda_i\lambda_j} - \frac{4}{3}\left(\frac{(I_1-\lambda_j^2)\lambda_j}{\lambda_i}+\frac{(I_1-\lambda_i^2)\lambda_i}{\lambda_j}\right)\right.\\ & \left. + \delta_i^j\left(2(I_1-\lambda_i^2)+\frac{4}{3}\frac{I_2}{\lambda_a^2}\right) + \Big(1-\delta_i^j\Big)\lambda_i\lambda_j\right)\\ & + \frac{K}{\lambda_i\lambda_j\beta}\Big(\beta J^{-\beta}+\delta_i^j\Big(J^{-\beta}-1\Big)\Big).\end{aligned} \tag{B.13}$$

References

[1] M. C. Boyce, E. M. Arruda, Constitutive models of rubber elasticity: A review (jul 2000). doi:10.5254/1.3547602.
URL https://meridian.allenpress.com/rct/article/73/3/504/92749/Constitutive-Models-of-Rubber-Elasticity-A-Review

[2] P. Steinmann, M. Hossain, G. Possart, Hyperelastic models for rubber-like materials: Consistent tangent operators and suitability for Treloar's data, Archive of Applied Mechanics 82 (9) (2012) 1183–1217. doi:10.1007/s00419-012-0610-z.

[3] C. O. Horgan, J. G. Murphy, Limiting chain extensibility constitutive models of Valanis-Landel type, Journal of Elasticity 86 (2) (2007) 101–111. doi:10.1007/s10659-006-9085-x.

[4] H. Darijani, R. Naghdabadi, Hyperelastic materials behavior modeling using consistent strain energy density functions, Acta Mechanica 213 (3-4) (2010) 235–254. doi:10.1007/s00707-009-0239-3.

[5] F. Gruttmann, R. L. Taylor, Theory and finite element formulation of rubberlike membrane shells using principal stretches, International Journal for Numerical Methods in Engineering 35 (5) (1992) 1111–1126. doi:10.1002/nme.1620350511.
URL https://doi.org/10.1002/nme.1620350511

[6] J. C. Simo, R. L. Taylor, Quasi-incompressible finite elasticity in principal stretches. continuum basis and numerical algorithms, Computer Methods in Applied Mechanics and Engineeringdoi:10.1016/0045-7825(91)90100-K.

[7] G. Duffett, B. D. Reddy, The analysis of incompressible hyperelastic bodies by the finite element method, Computer Methods in Applied Mechanics and Engineering 41 (1) (1983) 105–120. doi:10.1016/0045-7825(83)90055-5.

[8] Y. Başar, M. Itskov, Finite element formulation of the Ogden material model with application to ruber-like shells, International Journal for Numerical Methods in Engineeringdoi:10.1002/(SICI)1097-0207(19980815)42:7<1279::AID-NME437>3.0.CO;2-I.

[9] G. A. Holzapfel, R. Eberlein, P. Wriggers, H. W. Weizsäcker, Large strain analysis of soft biological membranes: Formulation and finite element analysis, Computer Methods in Applied Mechanics and Engineering 132 (1-2) (1996) 45–61. doi:10.1016/0045-7825(96)00999-1.

[10] J. Kiendl, K.-U. Bletzinger, J. Linhard, R. Wüchner, Isogeometric shell analysis with Kirchhoff–Love elements, Computer Methods in Applied Mechanics and Engineering 198 (49-52) (2009) 3902–3914. doi:10.1016/J.CMA.2009.08.013.
URL https://www-sciencedirect-com.tudelft.idm.oclc.org/science/article/pii/S0045782509002680?{_}rdoc=1{&}{_}fmt=high{&}{_}origin=gateway{&}{_}docanchor={&}md5=b8429449ccfc9c30159a5f9aeaa92ffbhttps://www.sciencedirect.com/science/article/pii/S0045782509002680{#}fig18http://li

[11] J. Kiendl, Y. Bazilevs, M.-C. Hsu, R. Wüchner, K.-U. Bletzinger, The bending strip method for isogeometric analysis of Kirchhoff–Love shell structures comprised of multiple patches, Computer Methods in Applied Mechanics and Engineering 199 (37-40) (2010) 2403–2416. doi:10.1016/J.CMA.2010.03.029.
URL http://linkinghub.elsevier.com/retrieve/pii/S0045782510001064https://www.sciencedirect.com/science/article/pii/S0045782510001064?via{%}3Dihub

[12] J. Kiendl, M.-C. Hsu, M. C. Wu, A. Reali, Isogeometric Kirchhoff–Love shell formulations for general hyperelastic materials, Computer Methods in Applied Mechanics and Engineering 291 (2015) 280–303. doi:10.1016/J.CMA.2015.03.010.
URL https://www-sciencedirect-com.tudelft.idm.oclc.org/science/article/pii/S0045782515001127?{_}rdoc=1{&}{_}fmt=high{&}{_}origin=gateway{&}{_}docanchor={&}md5=b8429449ccfc9c30159a5f9aeaa92ffb

[13] T. J. Hughes, J. A. Cottrell, Y. Bazilevs, Isogeometric analysis: CAD, finite elements, NURBS, exact geometry and mesh refinement, Computer Methods in Applied Mechanics and Engineering 194 (39-41) (2005) 4135–4195. arXiv:1608.04366, doi:10.1016/j.cma.2004.10.008.
URL http://linkinghub.elsevier.com/retrieve/pii/S0045782504005171https://www.sciencedirect.com/science/article/pii/S0045782504005171{#}fig1

[14] A. B. Tepole, H. Kabaria, K.-U. Bletzinger, E. Kuhl, Isogeometric Kirchhoff–Love shell formulations for biological membranes, Computer Methods in Applied Mechanics and Engineering 293 (2015) 328–347. doi:10.1016/J.CMA.2015.05.006.
URL https://www.sciencedirect.com/science/article/pii/S0045782515001723

[15] F. Roohbakhshan, R. A. Sauer, Efficient isogeometric thin shell formulations for soft biological materials, Biomechanics and Modeling in Mechanobiology 16 (5) (2017) 1569–1597. doi:10.1007/s10237-017-0906-6.
URL http://link.springer.com/10.1007/s10237-017-0906-6

[16] S. Morganti, F. Auricchio, D. J. Benson, F. I. Gambarin, S. Hartmann, T. J. Hughes, A. Reali, Patient-specific isogeometric structural analysis of aortic valve closure, Computer Methods in Applied Mechanics and Engineering 284 (2015) 508–520. doi:10.1016/j.cma.2014.10.010.
URL https://www-sciencedirect-com.tudelft.idm.oclc.org/science/article/pii/S0045782514003806

[17] M. C. Wu, R. Zakerzadeh, D. Kamensky, J. Kiendl, M. S. Sacks, M.-C. Hsu, An anisotropic constitutive model for immersogeometric fluid–structure interaction analysis of bioprosthetic heart valves, Journal of Biomechanics 74 (2018) 23–31. doi:10.1016/J.JBIOMECH.2018.04.012.
URL https://www.sciencedirect.com/science/article/pii/S0021929018302768

[18] D. Kamensky, M.-C. Hsu, D. Schillinger, J. A. Evans, A. Aggarwal, Y. Bazilevs, M. S. Sacks, An immersogeometric variational framework for fluid–structure interaction: Application to bioprosthetic heart valves, Computer Methods in Applied Mechanics and Engineering 284 (2015) 1005–1053. doi:10.1016/J.CMA.2014.10.040.
URL https://www.sciencedirect.com/science/article/pii/S0045782514004101

[19] M. C. Hsu, D. Kamensky, F. Xu, J. Kiendl, C. Wang, M. C. Wu, J. Mineroff, A. Reali, Y. Bazilevs, M. S. Sacks,

Dynamic and fluid–structure interaction simulations of bioprosthetic heart valves using parametric design with T-splines and Fung-type material models, Computational Mechanics 55 (6) (2015) 1211–1225. arXiv:15334406, doi:10.1007/s00466-015-1166-x.
URL http://link.springer.com/10.1007/s00466-015-1166-x

[20] F. Xu, S. Morganti, R. Zakerzadeh, D. Kamensky, F. Auricchio, A. Reali, T. J. R. Hughes, M. S. Sacks, M.-C. Hsu, A framework for designing patient-specific bioprosthetic heart valves using immersogeometric fluid-structure interaction analysis, International Journal for Numerical Methods in Biomedical Engineering 34 (4) (2018) e2938. doi:10.1002/cnm.2938.
URL http://doi.wiley.com/10.1002/cnm.2938

[21] M. C. Hsu, D. Kamensky, Y. Bazilevs, M. S. Sacks, T. J. Hughes, Fluid–structure interaction analysis of bioprosthetic heart valves: significance of arterial wall deformation, Computational Mechanics 54 (4) (2014) 1055–1071. doi:10.1007/s00466-014-1059-4.
URL /pmc/articles/PMC4286305/?report=abstracthttps://www.ncbi.nlm.nih.gov/pmc/articles/PMC4286305/

[22] A. J. Herrema, E. L. Johnson, D. Proserpio, M. C. Wu, J. Kiendl, M.-C. Hsu, Penalty coupling of non-matching isogeometric Kirchhoff–Love shell patches with application to composite wind turbine blades, Computer Methods in Applied Mechanics and Engineering 346 (2019) 810–840. doi:10.1016/J.CMA.2018.08.038.
URL https://www.sciencedirect.com/science/article/pii/S0045782518304365?via{%}3Dihub

[23] Y. Bazilevs, M.-C. Hsu, J. Kiendl, R. Wüchner, K.-U. Bletzinger, 3D simulation of wind turbine rotors at full scale. Part II: Fluid-structure interaction modeling with composite blades, International Journal for Numerical Methods in Fluids 65 (1-3) (2011) 236–253. doi:10.1002/fld.2454.
URL http://doi.wiley.com/10.1002/fld.2454

[24] G. Holzapfel, Nonlinear solid mechanics: A continuum approach for engineering, John Wiley & Sons, ltd., 2000. arXiv:arXiv:1511.03484v1, doi:10.1023/A:1020843529530.

[25] P. Wriggers, Nonlinear finite element methods, 2008. arXiv:arXiv:1011.1669v3, doi:10.1007/978-3-540-71001-1.

[26] Y. Başar, D. Weichert, Nonlinear Continuum Mechanics of Solids, Springer-Verlag Berlin Heidelberg GmbH, 2013. doi:10.1007/978-3-662-04299-1.

[27] R. A. Sauer, T. X. Duong, On the theoretical foundations of thin solid and liquid shells, Mathematics and Mechanics of Solids 22 (3) (2017) 343–371. doi:10.1177/1081286515594656.

[28] M. Mooney, A theory of large elastic deformation, Journal of Applied Physicsdoi:10.1063/1.1712836.

[29] R. S. Rivlin, Torsion of a rubber cylinder, Journal of Applied Physics 18 (5) (1947) 444–449. doi:10.1063/1.1697674.
URL http://aip.scitation.org/doi/10.1063/1.1697674

[30] P. J. Flory, Thermodynamic relations for high elastic materials, Transactions of the Faraday Societydoi:10.1039/TF9615700829.

[31] S. Klinkel, S. Govindjee, Using finite strain 3D-material models in beam and shell elements, Engineering Computations (Swansea, Wales) 19 (3-4) (2002) 254–271. doi:10.1108/02644400210423918.

[32] R. Ogden, Large deformation isotropic elasticity: on the correlation of theory and experiment for compressible rubberlike solids, Proceedings of the Royal Society of London. A. Mathematical and Physical Sciencesdoi:10.1098/rspa.1972.0096.

[33] J. C. Simo, C. Miehe, Associative coupled thermoplasticity at finite strains: Formulation, numerical analysis and implementation, Computer Methods in Applied Mechanics and Engineeringdoi:10.1016/0045-7825(92)90170-O.

[34] S. Doll, K. Schweizerhof, On the development of volumetric strain energy functions, Journal of Applied Mechanics, Transactions ASME 67 (1) (2000) 17–21. doi:10.1115/1.321146.

[35] S. Reese, S. Govindjee, A theory of finite viscoelasticity and numerical aspects, International Journal of Solids and Structures 35 (26-27) (1998) 3455–3482. doi:10.1016/s0020-7683(97)00217-5.

[36] K. C. Valanis, R. F. Landel, The strain-energy function of a hyperelastic material in terms of the extension ratios, Journal of Applied Physicsdoi:10.1063/1.1710039.

[37] B. Jüttler, U. Langer, A. Mantzaflaris, S. E. Moore, W. Zulehner, Geometry + Simulation Modules: Implementing Isogeometric Analysis, PAMM 14 (1) (2014) 961–962. doi:10.1002/pamm.201410461.
URL http://doi.wiley.com/10.1002/pamm.201410461

[38] L. R. G. Treloar, The Physics of Rubber Elasticity, 1st Edition, Oxford University Press, Oxford, UK, 1975.

[39] J. Chopin, A. Panaitescu, A. Kudrolli, Corner singularities and shape of stretched elastic sheets, Physical Review E 98 (4) (2018) 043003. doi:10.1103/PhysRevE.98.043003.
URL https://link.aps.org/doi/10.1103/PhysRevE.98.043003

[40] N. Büchter, E. Ramm, D. Roehl, Three-dimensional extension of non-linear shell formulation based on the enhanced assumed strain concept, International Journal for Numerical Methods in Engineering 37 (15) (1994) 2551–

2568. doi:10.1002/nme.1620371504.

[41] B. Brank, J. Korelc, A. IbrahimbegoviĆ, Nonlinear shell problem formulation accounting for through-the-thickness stretching and its finite element implementation, Computers and Structures 80 (9-10) (2002) 699–717. doi:10.1016/S0045-7949(02)00042-1.

[42] M. Schwarze, S. Reese, A reduced integration solid-shell finite element based on the EAS and the ANS concept-Large deformation problems, International Journal for Numerical Methods in Engineering 85 (3) (2011) 289–329. doi:10.1002/nme.2966.

[43] H. Verhelst, M. Möller, J. den Besten, M. Kaminski, F. Vermolen, Equilibrium Path Analysis Including Bifurcations with a Fully-Integrated Arc-Length Method Avoiding A Priori Perturbations (accepted for publication), in: Proceedings of ENUMATH2019 Conference, Egmond aan Zee, The Netherlands, 2020.